REPORT SERIES IN AEROSOL SCIENCE
N:o 187 (2016)

ON GAS-PHASE SYNTHESIS OF NANOPARTICLES FOR ADVANCED ENERGY SOLUTIONS

TOMMI KARHUNEN

Faculty of Science and Forestry
University of Eastern Finland
Kuopio, Finland

Academic dissertation

To be presented, with the permission of the Faculty of Science and Forestry of the University of Eastern Finland, for public examination in Auditorium SN200, Snellmania Building at University of Eastern Finland, Kuopio, on August 16th, 2016, at 12 o'clock noon.

Kuopio 2016

Author's Address: Fine Particle and Aerosol Technology Laboratory
University of Eastern Finland
Department of Environmental and Biological Sciences
P.O. Box 1627
FI-70211 Kuopio, Finland
e-mail: tommi.karhunen@uef.fi

Supervisors: Professor Jorma Jokiniemi, Ph.D.
Department of Environmental and Biological Sciences
University of Eastern Finland

Docent Anna Lähde, Ph.D.
Department of Environmental and Biological Sciences
University of Eastern Finland

Reviewers: Professor Jyrki Mäkelä, Ph.D.
Department of Physics
Tampere University of Technology

Professor Tanja Kallio, Ph.D.
Department of Chemistry
Aalto University

Opponent: Karsten Wegner, Ph.D.
Institute of Process Engineering
Swiss Federal Institute of Technology (ETH) Zurich

ISBN 978-952-7091-58-6 (printed version)
ISSN 0784-3496
Helsinki 2016
Yliopistopaino

ISBN 978-952-7091-59-3 (pdf version)
http://ethesis.helsinki.fi
Helsinki 2016
Helsingin yliopiston verkkojulkaisut

Acknowledgements

This thesis is based on work carried out in the Fine Particle and Aerosol Technology group, Department of Environmental and Biological Sciences, University of Eastern Finland.

I would like to extend my deepest gratitude to my principle supervisor Professor Jorma Jokiniemi, Ph.D., for the opportunity to carry out cutting edge research on an interesting topic. Your guidance and understanding have been greatly appreciated, and I am indebted to you for your efforts to secure funding in these difficult times. Likewise, I would like to thank my second supervisor Docent Anna Lähde, Ph.D., for her support and advice over the years. Your help with the practical aspects, as well as all things chemical in nature, have been invaluable in the conclusion of this work.

I would also like to express my gratitude to the official reviewers of this thesis, Professor Jyrki Mäkelä, Ph.D., and Professor Tanja Kallio, Ph.D. for their constructive feedback and insightful comments on the work presented herein. I am also grateful to Lecturer Karsten Wegner, Ph.D., for kindly accepting the invitation to serve as an opponent in the public examination of the thesis.

I wish to extend my thanks to the head of the department, Professor Maija-Riitta Hirvonen, for the opportunity to work at the department, and for her tireless work on locating funding that enabled the completion of the thesis. I am also grateful to Kari Kuuspalo for his faith in me when I first arrived in the group, and for introducing me to the secrets of aerosol science.

My thanks also go to all my co-authors for their excellent work during our collaborations on the work presented in this thesis. Similarly, I am thankful to all my colleagues at the Fine Particle and Aerosol Technology group, both past and present, for providing a pleasant and stimulating working environment.

I am also grateful to my steadfast friends Maija and Petri Ihantola, Iiro Anttila and Aki Rissanen for their encouragements and the engaging discussions that have spurred my interest in science. Finally, I would like to express my warmest gratitude to my parents for their endless support and faith in me throughout the long road that led to the completion of this work.

The research presented in this thesis was financially supported by the University of Eastern Finland, the Fortum Foundation, the Foundation for Research of Natural

Resources in Finland, the Finnish Funding Agency for Technology and Innovation, the Kuopio University Foundation, and the Finnish Cultural Foundation. I am grateful to them all for making this thesis work possible.

Kuopio, August 2016

Tommi Karhunen

Tommi Juha Tapani Karhunen
University of Eastern Finland, 2016

Abstract

This Doctoral Thesis is on gas-phase synthesis of nanoparticles for advanced energy solutions. It covers the nanoparticle formation mechanisms in gas-phase processes based on aerosol techniques, the relationship of the synthesis conditions on the physical and chemical properties of the nanoparticulate material, as well as the relationship of the particulate properties on the performance of the materials in energy storage applications.

First, previous work and theoretical background of aerosol science, nanoparticle synthesis, and Li-ion secondary cell energy storage applications are introduced. Second, the nanoparticle synthesis and characterisation techniques utilised in the current work are described in greater detail. Also the method for the testing of suitability of the synthesised materials for the Li-ion battery application is defined. Lastly, the results of the experimental work are detailed and discussed.

The work has provided new knowledge on the gas-phase synthesis of several nanoparticulate materials using spray pyrolysis and flame spray pyrolysis techniques. The techniques provide simple, one-step processes for synthesis of nanoparticles with well defined characteristics. Furthermore, it was shown that these characteristics can be tuned by varying the synthesis parameters, such as reaction atmosphere, temperature, residence time, and stoichiometry.

In addition, it was observed that the properties of the produced nanomaterials have a significant impacts on their utility in the chosen application. This allows for optimisation of the synthesis conditions for the requirements of the application.

The spray pyrolysis process was used to produce homogeneous gold nanoparticles less than 5 nm in size. A designer precursor of homoleptic gold molecular clusters were used for the synthesis. The precursor was found to decompose and form surface stabilised, spherical cold nanoparticles, with the evaporating solvent droplets acting as microreactors.

The same process was found to work also for precursors consisting of industrial by-product $FeSO_4$ in the synthesis $LiFePO_4$ nanoparticles. This proof-of-concept study highlighted the relationship between the synthesis conditions and the product properties. It was also seen that there often exists trade-offs between various product properties, which can be tuned by choosing appropriate synthesis conditions.

Also the flame spray pyrolysis technique was used in synthesis of nanoparticulate material in the gas-phase. It was found that $Li_4Ti_5O_{12}$ nanoparticles, both pure and doped with

conducting metal, can be obtained with a simple and fast single-step process. The standard set-up was found to produce material with very small crystallites which did not perform very well in the Li-ion battery application.

However, by adding a simple laminar flow furnace to the set-up the crystallite size was found to increase by about factor of four. As a result the product performance in Li-ion batteries underwent marked improvement showing specific capacities superior to commercially available alternatives, especially at high current operation. The $LiFePO_4/Li_4Ti_5O_{12}$ pair would make promising electrodes for next generation Li-ion batteries optimised for application where high peak power and long life time are required, for example electric construction machinery or local mass transit.

Keywords: Nanomaterials, Spray pyrolysis, Flame spray pyrolysis, Li-ion batteries

Contents

List of publications

This thesis consists of an introductory review, followed by 4 research articles. In the introductory part, these papers are cited according to their roman numerals.

I Lähde, A., Koshevoy, I., Karhunen, T., Torvela, T., Pakkanen, T. A., and Jokiniemi, J. (2014). Aerosol-assisted synthesis of gold nanoparticles, *J. Nanopart. Res.*, 16:2716.

II Karhunen, T., Torvela, T., Jokiniemi, J., and Lähde, A. (2014). Low-cost industrial by-products as precursors for $LiFePO_4$ synthesis, *J. Nanopart. Res.*, 16:2674.

III Karhunen, T., Lähde, A., Leskinen, J., Büchel, R., Waser, O., Tapper, U., and Jokiniemi, J. (2011). Transition Metal-Doped Lithium Titanium Oxide Nanoparticles Made Using Flame Spray Pyrolysis, *ISRN Nanotech.*, 2011:180821.

IV Karhunen, T., Välikangas, J., Torvela, T., Lähde, A., Lassi, U., and Jokiniemi, J. (2015). Effect of doping and crystallite size on the electrochemical performance of $Li_4Ti_5O_12$, *J. Alloys Comp.*, 659:132–137.

The original articles have been reproduced with permission from the copyright holders.

1 Introduction

1.1 Background and motivation

Engineered nanomaterials have become a core part of materials research and development in the recent decades (Gurav et al., 1993). When the dimensions of the material microscopic structure decrease to below 100 nm their chemical and physical properties undergo significant changes (Das and Ansari, 2009). For example, gold can be chemically active, ceramics can go from brittle to superelastic, and metals can become superparamagnetic (Ruusunen et al., 2015).

As such the production rates of nanomaterials have increased rapidly, with current estimates ranging from tens of thousands to millions of tons per year depending on what is included (Luther and Zweck, 2013). The nanomaterials can take many forms from bulk nanoceramics and nanocrystalline metals to one and two dimensional carbons structures (graphene and carbon nanotubes), as well as more complicated morphologies (e.g. tripods or stars) (Das and Ansari, 2009). However, one large subgroup is nanoparticulate materials; here defined consisting of solid particles with all dimensions below 100 nm, and possible agglomerated to larger structures.

For these the material properties depend strongly on the particle diameter (Das and Ansari, 2009). In particular, the smaller the particle size the greater the specific surface area is, leading to significantly increased surface reaction rates. This makes them ideal for many applications, including catalytic materials, sensors, supercapacitors and Li-ion batteries (du Pasquier et al., 2003; Pratsinis, 2010; Scrosati and Garche, 2010; Waser et al., 2011).

While these nanoparticulate materials can be synthesised using solid or solution based techniques, aerosol based processes have been found to particularly useful (Pratsinis, 2010). Their major advantages are simplicity, product purity, and absence of liquid by-products. Furthermore they afford excellent control of the products properties such as particle size, shape, composition, and crystallinity (Wang, 2004; Strobel and Pratsinis, 2007).

As such the aerosol based synthesis on nanoparticulate materials has found use in a number of applications ranging from additives and pigments through catalysts and sensors to energy generation and storage (Das and Ansari, 2009).

In the following work synthesis of metal and metal oxide nanoparticles using the aerosol based methods has been investigated. Various raw materials, ranging from industrial by-products to designed molecules, have been utilised as the precursors for the synthesis.

1.2 Objectives of the study

The overall objective of the study was to develop aerosol based nanoparticle synthesis methods for the production of advanced materials for next generation energy solutions. Spray pyrolysis and flame spray pyrolysis methods were chosen due to their simplicity, versatility in precursor materials, and ease of synthesis parameter control. The products chosen for the study were nanoparticulate electrode materials for Li-ion batteries, $Li_4Ti_5O_{12}$ and $LiFePO_4$. Also nanosized gold particles with interesting photonic properties were synthesised.

The specific goals of the study were:

- Development of a simple synthesis process for stable nanosized gold particles (Paper I)
- Development of a value-adding process of nanoparticles synthesis for high-tech applications from industrial by-product precursors (Paper II)
- Development of single-step process for the synthesis and doping of nanoparticulate electrode material for Li-ion battery (Papers III and IV)
- Optimisation of the synthesis conditions of the electrode material to achieve best electrochemical performance (Paper IV)

2 Scientific background

2.1 Aerosols: definitions and classification

A number of classifications are used for material suspensions depending on the homogeneity of the mixture and the phases of the materials involved, cf. Table 1 (Hinds, 1999; Atkins, 1990). Aerosols form a subclass of the suspensions where the dispersion medium is gaseous and the dispersed phase either liquid or solid. The particle size of the dispersed phase of an aerosol is generally taken to range about 1 nm to 10s of µm's. Below this range the particles are usually considered molecular clusters, while above the range they are so large that they do not remain airborne for significant periods.

Table 1: Classifications of suspensions.

Dispersion medium	Dispersed phase: Gas	Liquid	Solid
Gas	*	Liquid aerosol	Solid aerosol
Liquid	Foam	Emulsion	Sol[a] Suspension
Solid	Sponge	Gel	Solid sol[a] Granular mixture

* Gases are always miscible

[a] Colloid: particle size of dispersed phase less than about 500 nm

The aerosol particles are usually size classified further to various modes as shown in Table 2 (Friedlander, 2000). The largest size fraction, referred to as the coarse mode, is mainly a result of mechanical processes such as dust raised by wind or roadways degraded by vehicle traffic. Particles in this size fraction are also synthesised by grinding solids, or solid mixtures. The mode generally peaks around particle size of about 10 µm. The airborne residence times of the coarse mode particles depend heavily on the turbulent mixing of the aerosol, ranging in the lower troposphere from a few hours for 50 µm particles to couple of days for 2.5 µm ones.

The next mode is called the accumulation mode as particles seem to accumulate at this size range (Friedlander, 2000). On one hand, smaller particles grow to these sizes

Table 2: Size classifications of aerosol particles.

Size class	Size range
Coarse mode	$> 2.5\mu$m
Accumulation mode	100 nm – 2.5 μm
Nucleation mode	< 100nm

through physico-chemical processes, such as condensation and coagulation. On the other hand, particle removal processes tend to be weakest within the range. Due to this combination the mode peaks around 300 nm. This is also the size range where particle collection and detection is generally very challenging. Synthetic aerosol particles in this size range tend to be agglomerates of smaller primary particles, but can also be generated from liquid droplets by e.g. spray drying.

Finally, there is the nucleation, or ultrafine, mode. This size range is mainly composed of particles produced locally through gas-to-particle conversion (Friedlander, 2000), resulting from e.g. combustion or photochemical activity. Also primary particles synthesised using gas-phase or aerosol phase methods are generally ultrafine particles. These small particles tend to be efficiently removed by attachment to the accumulation mode particles. The characteristic residence time for the nucleation mode particles is given by Equation 1, and turns out to be about 80 minutes for typical ambient air, or about 0.1 s in a case of aerosol synthesis of engineered nanoparticles (Kodas and Hampden-Smith, 1999).

$$\tau = \frac{1}{2\pi D \bar{d}_p a N_a c} \tag{1}$$

The sources of aerosols are varied and depend on the circumstances. In material synthesis aerosol methods have been found to be efficient means of producing nanosized products (Kodas and Hampden-Smith, 1999; Kammler et al., 2001). As such there are seeing wide spread adoption in various material applications, e.g. medical compounds, pigments, additives, as well as coatings and nanocomposites. There are also other anthropogenic sources such as particles emitted from combustion processes, nucleation and ageing of gaseous emissions from vehicles and industry, and course particles generated by human activity (e.g. soil tilling, construction). Finally, natural processes ranging from photochemical activation of organic gasses released by plans to ash ejected by

volcanic activity and dust raised by strong winds produce aerosol particles (Seinfield and Pandis, 1998).

2.2 Nucleation and growth of aerosol particles

The formation of new aerosol particle nuclei takes place through a gas-to-particle conversion (Seinfield and Pandis, 1998). This process is composed of several steps (Spurny, 2000): i) reactions of gas molecules, ii) nucleation of vapours, iii) vapour condensation onto existing particles, iv) reactions on the particle surfaces, and v) reactions/ordering of molecules within the particles. Each of these steps can act as a rate-determining process in the particle formation and growth (Seinfield and Pandis, 1998).

The reactions of gas molecules result from collisional interaction between the molecules and depends on the gas properties such as temperature, pressure and density (Mädler and Friedlander, 2007). These reactions push the system towards an equilibrium state defined by a minimum in the Gibbs free energy (Bale et al., 2002).

If the chemical reactions produce species with sufficiently low vapour pressure phase change from gas to liquid or solid might be energetically favoured (Donahue et al., 2009). A supersaturation condition (Seinfield and Pandis, 1998) of the gaseous species is realised due to the reactions, or a change in the surrounding conditions (e.g. cooling). This will then lead to nucleation of one (homogeneous or self-nucleation) or more (co-nucleation) gaseous species, a gas-to-particle conversion process(Friedlander, 2000; Mädler and Friedlander, 2007). In high-temperature reactions, e.g. flames, the supersaturation is reached during the subsequent cooling of the reaction gases, or due to generation of gaseous species with extremely low volatility (Sippula et al., 2012).

In addition to the self-nucleation, low vapour pressure species can undergo phase transitions via heterogeneous condensation into existing particles or surfaces. This can, in general, take place at lower supersaturation conditions (e.g. 1.3 for water condensation Ag nanoparticles (Porstendörfer et al., 1985)) than the homogeneous nucleation (4.2 for water) (Friedlander, 2000). Additional chemical reactions can also be induced by the presence of the particles, or other surface. These surface reactions may be simply mediated by the surfaces (catalysis) or may result in modification of the surface chemistry (Rodriguez et al., 2001). The reaction rates are controlled by the the rate of collisions between the gas molecules and the surface. This rate in turn depends on the

surface area present meaning for catalytic application small particles would be more efficient (Seinfield and Pandis, 1998).

Finally, chemical reactions can take within the volume of the particles. This can be a result of interaction with gaseous molecules, in which case the reactions proceed from the surface inward (Ma et al., 2013). Alternatively there might be reactions between various species or polymorphs within the particles. Typically the gas-to-particle process results initially in amorphous or nanocrystalline particles which then undergo as a solid state process a molecular re-ordering, i.e. crystal formation (Ma et al., 2013). These solid state processes tend to have slower rates than the reactions involving gas molecules due to the comparatively slow diffusion rates (10^{-7} to 10^{-15} cm^2/s for solids compared 10^{-1} cm^2/s for gases) (Kodas and Hampden-Smith, 1999).

When the nucleation is sufficiently rapid high primary particle concentration will be achieved. Under these conditions collisions between the primaries will result in coagulation of the particles into larger agglomerate structures (Friedlander, 2000). This coagulation rate is a function of the particle concentration. In general, molecular re-ordering will lead to the coalescence, or sintering, of the loose agglomerates into denser aggregates, or even to solid, spherical particles (Lehtinen et al., 1996).

The form of the final aerosol particles depends on the relative rates of the coagulation and coalescence(Friedlander, 2000). When coagulation is significantly faster loose agglomerates should be expected, while when coalescence rate dominates spherical particles will be generated. While the coagulation rate is independent of temperature, the rate of the coalescence is higher when the particle temperature is high. As such there can be situations when initially coalescence dominates leading to spherical particles, but once the aerosol cools (e.g. after quenching) coagulation takes over and leads to agglomerates of the spherical particles. Often, in such cases, the spherical particles are called primary particles even though they themselves might be composed of smaller domains as a residue of the original primary particles.

2.3 Gas-phase synthesis of nanoparticles

Nanoparticles have been synthesised using various methods which can, in general, be classified as solid, liquid or gas-phase routes. The solid-phase route includes mechanical milling and mechanochemical synthesis (Tjong and Chen, 2004). These are typically

low-cost and simple to implement. However, they suffer from large particles sizes and size distributions, as well as particle agglomeration (Pitkethy, 2003; Tjong and Chen, 2004); to achieve nanoparticles use of additives is required. Furthermore, impurities from the process equipment can contaminate the product.

The liquid-phase route involves chemical reactions in solution followed by filtering or spray drying to collect the resulting precipitate (Pitkethy, 2003). This flexible and inexpensive process can be used to generate a wide variety of compounds, and is widely used in, for example, medical industry. However, large liquid volumes, strict pH controls and low yields are common drawbacks of the method (Fotou et al., 2000; Lu et al., 2007; Pitkethy, 2003). In addition, solvent residues on bound to the product powder often require additional washing steps and may involve environmentally unfriendly solvents.

Gas-phase, or aerosol, routes have many advantages for nanoparticle synthesis. These include production of particles of high purity composed of non-porous primary particles with small sizes, and relatively narrow size distribution, as well as rapid and continuous production (Kruis et al., 1998; Kodas and Hampden-Smith, 1999; Kammler et al., 2001). Furthermore, the gas-phase reactions can be controlled to produce metastable products (Pratsinis, 2010). The gas-phase techniques are also, in general, energy and raw-material efficient and do not result in toxic slurries. These qualities make them excellent methods for cleantech applications. However, their disadvantages include difficulties in producing unagglomerated particles (Kammler et al., 2001).

A number of synthesis processes have been developed over the years and many of the parameters are well understood (Gurav et al., 1993; Kodas and Hampden-Smith, 1999; Swihart, 2003; Buesser and Pratsinis, 2012). The processes can, generally, be divided into flame and non-flame techniques. In both a continuous gas stream containing the precursor in either gaseous or aerosol form is fed into a reaction zone where the formation of the product phase takes place. Subsequently the stream is generally diluted to stop the reactions as well as particle growth and aggregation.

In the case of the non-flame techniques the reaction zone is usually a laminar or turbulent flow tube. The chemical reactions can be initiated by introducing a reacting gas, heat or radiation; alternatively particle formation can be achieved by altering the gas properties, for example by adiabatic cooling (Gurav et al., 1993; Kodas and Hampden-Smith, 1999). The most common technique is probably to use a laminar flow

furnace that is heated to a temperature where the reactions between the precursors, or a precursor and the carrier gas takes place. These techniques would include inert gas condensation, pulsed laser ablation, spark discharge generation, ion sputtering, spray drying, spray pyrolysis, physical vapour synthesis, chemical vapour synthesis, laser pyrolysis/photothermal synthesis, thermal plasma synthesis (Swihart, 2003).

On the other hand, in the flame techniques the precursor stream is fed into a flame where the heat and/or the free radicals initiate the reactions leading to the product formation (Pratsinis, 1998). The flame can be a result of the the combustion of the precursor solvent, or a separate flame (Mäkelä et al., 2004; Strobel and Pratsinis, 2007). This class would contain e.g. flame spray pyrolysis, flame assisted spray pyrolysis, vapour-fed aerosol flame synthesis, liquid flame Spray.

2.3.1 Physical vapour synthesis and deposition

In physical vapour synthesis (PVS), or deposition (PVD), a supersaturation of a gaseous product species is obtained by altering the properties of the gas, usually by cooling it (Arai, 1996). The product gas is often generated by first vaporising solid metallic or non-metallic precursor in an evaporation zone of the reactor, though joule heating, spark generation or laser ablation, for example. The gas is then lead to a colder condensation zone where particle formation through nucleation takes place. In such systems the process is sometime referred to as evaporation-condensation technique, for obvious reason. In PVS the product powder is then collected while in PVD the nuclei, or the vapour, are deposited onto an existing surfaces or particles.

The PVS system is extremely simple and can be used to produce nanoparticles with very well defined particle size (Gracia-Pinilla et al., 2010). However, the range of product materials are limited by the availability of precursors that can be evaporated at the temperature of the evaporation zone and brought to supersaturation condition in the condensation zone.

2.3.2 Chemical vapour synthesis and deposition

Chemical vapour synthesis (CVS), or condensation, is a gas-phase nanoparticle synthesis method where gaseous precursors are introduced into a, typically, heated reaction

zone such as a laminar flow furnace (Arai, 1996). Here the gaseous compounds undergo chemical reactions, such as decomposition, which results in a supersaturation of the product compound. The product will then rapidly nucleate to form the product particles (Chang et al., 1994). To stop undesired agglomeration and sintering the product aerosol is, in general, subsequently quenched with cool, particle free gas.

Chemical vapours deposition (CVD) is a similar process but instead of self-nucleation the product vapour undergoes heterogeneous condensation onto an existing surface, or particles to produce shape controlled materials or thin films (Arai, 1996). Both the CVS and CVD offer flexibility in product material and the choice of the precursors. The precursors can be gaseous (e.g. SiH_4), or alternatively solid or liquid as long as they can be volatilised prior to the reactions in the reaction zone of the reactor. This can be achieved through the use of bubblers and sublimation sources, or evaporation of dispersed precursor solution droplets (Swihart, 2003).

2.3.3 Spray pyrolysis

The technique is an atmospheric pressure aerosol assisted particle synthesis process (Hampden-Smith et al., 2006). The reactor consists of a heated evaporation and reaction zone within a laminar flow oven (Lähde et al., 2011) and a quenching and dilution zone, generally, within a porous tube diluter (Lyyränen et al., 2004). The precursor solution is aerosolised using, for example, an ultrasonic nebuliser (RBI Pyrosol 7901) and the produced droplets carried into the reactor with a carrier gas.

In the heated zone the solvent evaporates and the precursor undergoes reactions that generate the product compounds. The type of reactions and the resulting compounds can be controlled though the selection of the carrier gas, leading to oxidation, reduction, or thermal decomposition of the precursors (Gurav et al., 1993).

Aside from the chemical reaction environment the reactions can be controlled by varying the reaction zone temperature and residence time (Gurav et al., 1993). At low temperatures the solvent evaporation and dissociation of the precursor is slow meaning any chemical reaction will likely take place within the droplet at or below the boiling point of the solvent. There might also be insufficient time at the elevated temperatures for molecular rearrangement within the formed particles leading to amorphous or nanocrystalline product, especially for products with large molecules such as medical

compounds (Lähde et al., 2008).

On the other hand, at high temperatures the solvent will evaporate quickly giving the dry particles longer residence at the elevated temperatures, which can lead to further chemical reactions as well as sintering. This will in general result in solid, single-crystalline particles. Furthermore, at different temperatures the reaction end points (e.g. polymorphs) can vary due to the balance between enthalpy and entropy.

The aerosol exiting the heated zone is rapidly cooled with a large volume of dilution gas (e.g. air, or N_2) (Lähde et al., 2011). This reduces the aerosol concentration and halts the sintering of the particles. Thus the size of the primary particles and the degree of agglomeration can be controlled. Also chemical reactions will stop allowing formation of metastable phases.

2.3.4 Flame spray pyrolysis

In FSP the precursor solution is fed through a capillary in the middle of the device (Mädler et al., 2002). The liquid feed is then atomised with high-pressure dispersion gas fed through an annular aperture around the capillary tube; the droplet size is determined by the dispersion gas flow rate.

A premixed methane-oxygen flamelet ignites the aerosolised precursor solution resulting in the formation of a high-temperature flame, with temperatures in excess of 2000 K (Mädler et al., 2002; Gröhn et al., 2014), within which the organic parts of the precursor and the solvent the will undergo complete combustion, forming carbon dioxide and water vapour.

The metallic or semi-metallic components of the precursor will then nucleate and condensate to form primary particles of pure metals or metal salts or metal oxides (Strobel and Pratsinis, 2007). Various crystallite shapes and particle morphologies can be obtained depending on the precursors and synthesis conditions, as illustrated by Figure 1.

Some aggregation will take place in the high-temperature region of the flame where coalescence is rapid leading to primary particle growth. However, the quenching of the particle sintering is very efficient (Strobel and Pratsinis, 2007) due to radiation and convection. Thus the sintering will quickly stop and the primary particle size will remain small (down to 10 nm).

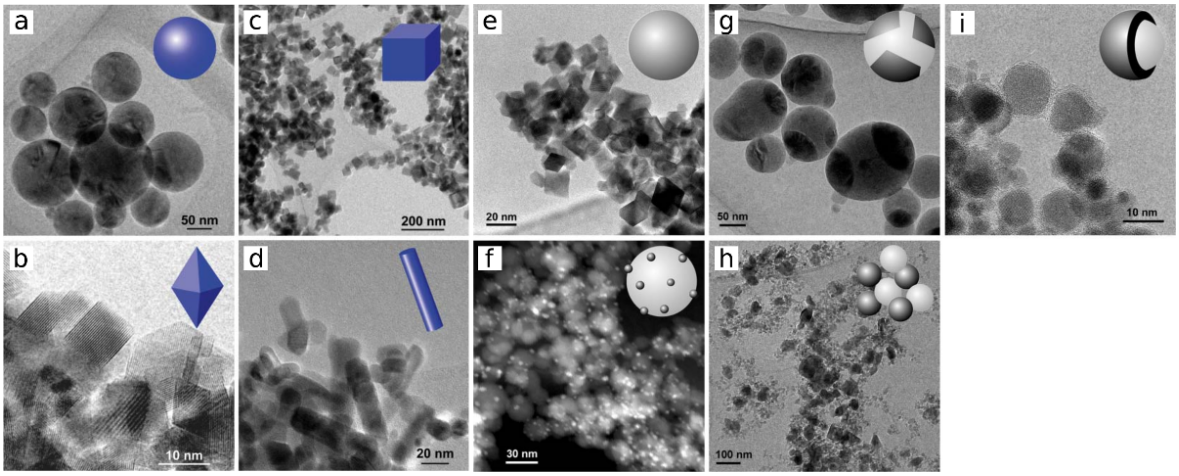

Figure 1: Schematics and TEM examples of various FSP synthesised crystallites (a-d) and particle morphologies (e-i) (adapted from Strobel and Pratsinis (2007)).

However, the quenching will also stop the growth and ordering of the crystallite structures, possibly leading to metastable polymorphs or multi-crystalline particles. This can be controlled to a point with a proper selection the combustion enthalpy or restriction of the air entrainment.

Downstream of the flame further agglomeration of the primary particles will take place due to a high particle concentration. However, in the standard FSP process the temperature in this region is sufficiently low to prevent further coalescence, or re-ordering of the crystalline structure.

2.4 Engineered nanomaterials

Engineered nanomaterials are generally defined as synthetic compounds with at least one structural dimension smaller than 100 nm (Nel et al., 2006). For sheet-like nanomaterials this would be the thickness, while for tubes, ribbons and fibres, and for nanoparticles there would be two and three nano dimensions, respectively. Nanomaterials are of interest in material industry as, at the nanoscale, so called size effects can lead to drastic changes in several material properties, such as melting and boiling points, dielectric constants, magnetic properties, surface energies, interaction with light, dispersibility, and mechanical strength (Hosokawa et al., 2008; Wang, 2004). The nanoparticulate materials will also tend to have very high specific surface areas

(in excess of 1000 m^2/g for activated carbon (Sun et al., 2007)).

These changes mean nanomaterials may have properties with suitability superior to the corresponding bulk materials in many applications. In addition several specific particle shapes can be synthesised, for example nanodots, nanorods, nanodisks, tri- and tetrapods, nanoneedles, nanoflowers, nanowires and -ribbons, nanotubes, nanofilms, as well as solid and hollow spherical nanoparticles (Das and Ansari, 2009; Miettinen et al., 2014; Strobel and Pratsinis, 2007).

On the other hand, many nanomaterials suffer from poor stability particularly at elevated temperatures and decreased inter-particular cohesion. Furthermore, nanoparticles released by the synthesis or degradation of nanomaterials may pose dangers to the environment and to human health due to enhanced permeation and retention in biological tissues caused by their small size (Oberdörster et al., 2005; Fang et al., 2011). These issues make the handling of nanomaterials more difficult (Hosokawa et al., 2008).

While various solid and solution-phase technologies are also used, aerosol techniques are an important route for commercial nanoparticulate products (Pratsinis, 2010), with production rates of millions of tons per year (Gurav et al., 1993). The major advantages of the aerosol-phase synthesis methods are simplicity, product purity, and absence of liquid by-products (Pratsinis, 2010). They are also capable of producing a extensive range of products, including carbon black, fumed silica, titania pigments, optical fibres, mixed metal oxides, metal salts, catalytic noble metals (Mädler and Friedlander, 2007; Strobel and Pratsinis, 2007).

Furthermore, the aerosol methods afford an excellent control of the product properties such as specific surface area, morphology, chemical and polymorph composition, as well as degree of crystallinity (Wang, 2004; Strobel and Pratsinis, 2007). As such they have found use in numerous applications including additives, pigments, catalysts, photochemistry, sensors, and tagging, as well as optical, electronic and magnetic devices (Das and Ansari, 2009).

For example gold nanoparticles can be utilised in photonics to manipulate the propagation, intensity and polarization of light (Zhou et al., 2011). They also exhibits the surface plasmon resonance characteristic resulting form a collective oscillation of the conducting electrons (de la Garza et al., 2010). As such they are being investigated for use in biotechnology, energy generation and storage and information technology applications (Wu et al., 2008).

One application of particulate relevance for this study is rechargeable Li-ion secondary cells (referred to as Li-ion batteries henceforth). The large specific surface area of nanoparticles allows for rapid charge-transfer between the electrodes and the electrolyte within the cells leading to high-current densities. Furthermore, for some materials of interest as targets of lithium intercalation reactions the bulk conductivity is insufficient for application in the batteries. However, as the particle size is reduced to the nanoscale the poor conductivity can be circumvented.

2.5 Lithium ion batteries

2.5.1 Structure and operating principles

Lithium-ion batteries have seen a rapid expansion in utilisation over the past decades due to their excellent specific energy (c. 100-150 Wh/kg) reaching market volumes in the billions of units annually (Scrosati and Garche, 2010). A conventional Li-ion battery (shown in Figure 2) has graphite (mesocarbon microbeads, MCMB) as the anode and lithium cobalt oxide ($LiCoO_2$) as the cathode.[1]

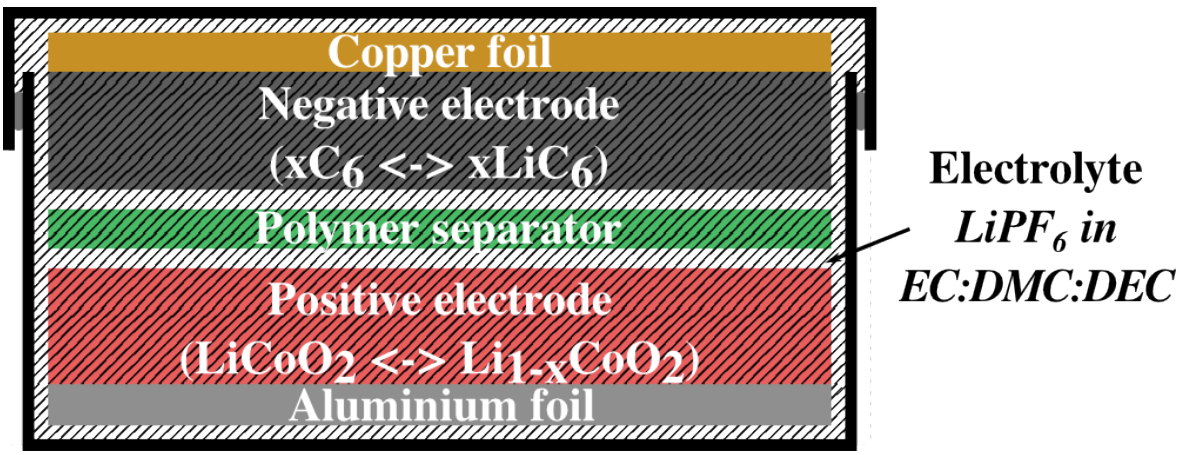

Figure 2: Schematic of one typical Li-ion battery structure. The half reactions at the negative and positive electrodes are also shown.

The electrical contact between the electrodes is generally prevented by a polymer fi-

[1]Although the terms anode and cathode do not strictly apply to rechargeable cells they will be used here for the sake of brevity, for the negative and positive electrodes or their intercalation active components, respectively.

brous filter separator. However, to allow for the diffusion of the Li-ions the separator is wetted by an electrolyte, usually consisting of a lithium salt (e.g. $LiPF_6$) in organic solvent (e.g. mixture of ethylene carbonate, dimethyl carbonate and/or diethyl carbonate) (Scrosati and Garche, 2010; Park et al., 2010).

During charging of the cell an external voltage is applied between the electrodes leading to current from the anode to the cathode (Scrosati and Garche, 2010; Park et al., 2010). This forces electrons to flow in the opposite direction, and raises the potential at the cathode and lowers it at the anode. The change of the potential leads to shifting of the equilibrium point between the lithiated and delithiated phases of the active material. Thus Li-ions are extracted out of the electrode ($LiCoO_2 \longrightarrow Li_{1\text{-}x}CoO_2 + xLi^+ + xe^-$). The Li-ions will then diffused across the electrolyte to the anode where they will intercalate between the graphite layers ($6\,xC + xLi^+ + xe^- \longrightarrow xLiC_6$).

Conversely, when the cell is discharging the Li-ions are leaving the anode and re-entering the cathode (Scrosati and Garche, 2010; Park et al., 2010). The ions diffuse across the electrolyte from the anode to the cathode while electrons flowing around the external wires complete the circuit. The reaction potentials at the negative and positive electrodes are about 0.3 and 4 V vs. Li/Li^+, respectively. This gives a total cell voltage of about 3.7 V which can be used to drive a load in the external circuit. For some electrode materials, such as $LiFePO_4$ or $Li_4Ti_5O_{12}$, the phase change can take place at nearly constant potential leading to a constant operating voltage.

2.5.2 Electrode materials

While the conventional Li-ion battery described above has found widespread success it does suffer from a number of drawbacks. First, there is a mismatch of the electrode reactions potentials compared to the stability range of the electrolyte (0.8 to 4.5 V vs. Li/Li^+) (Scrosati and Garche, 2010). At the potential of the reversible intercalation reaction at the anode also a decomposition of the electrolyte will take place. Fortunately, the decomposition products will form a so called solid electrolyte interface (SEI) layer on the surface of the anode. This leads to an initial irreversible capacity but does not prevent the normal operation of the battery; the SEI does not impede the Li-ion transport but does protect the electrolyte from the low potentials at the electrode.

The reaction potential at the cathode is just within the stability window of the elec-

trolyte (Scrosati and Garche, 2010). Thus under normal conditions the potential should stay below the oxidative threshold of the electrolyte. However, under unexpected events, such as overcharge, the potential might locally rise beyond the threshold leading to oxidation of the electrolyte. Unlike the decomposition at the anode this oxidation does not lead to a formation of a protective layer, as such the electrolyte oxidation can proceed unimpeded.

Overcharge protection is doubly important for $LiCoO_2$ cathode as the cathode material itself may decompose if too much lithium is removed from it (Scrosati and Garche, 2010). This leads to an irreversible oxygen evolution reaction: $3\,Li_{0.5}CoO_2 \longrightarrow Co_3O_4 + O_2 + 1.5\,Li^+ + 1.5\,e^-$ (Yoshio et al., 2009). The oxygen will then react with the electrolyte and generate heat. This can lead to a thermal runaway process where the excess heat leads to further oxygen evolution form the lithium cobalt oxide. In the worst case scenario the runaway may even cause the cell to explode due to the increased pressures (Jhu et al., 2012).

As a result extensive research has been conducted to locate alternative materials for the next generation Li-ion batteries. Although some promising alternative for the electrolyte have been suggested (e.g. polymer electrolytes and ionic liquids (Scrosati and Garche, 2010)) here we will concentrate on the electrode materials. An interesting possibility is to use a pair of electrode materials whose Li-ion insertion/extraction reactions take place within the stability window of the electrolyte. That way there is no risk irreversible electrolyte oxidation/reduction reactions. One such pair is $Li_4Ti_5O_{12}/LiFePO_4$ (Ohzuku et al., 1995; Panero et al., 2000; Ohzuku et al., 2001; Realea et al., 2004).

Both $Li_4Ti_5O_{12}$ (LTO) and $LiFePO_4$ (LFP) are lithium intercalation type electrodes and operate at about 1.5 and 3.5 V vs. Li/Li^+. This means there is no SEI formation at the anode and no electrolyte oxidation at the cathode. The LFP also does not suffer from collapse if too much lithium is extracted. Furthermore, the lattice size of both of the materials is virtually unchanged during the lithium intercalation reactions. As such there is no mechanical stresses on the material during electrochemical cycling which leads to excellent cycle lifetimes.

One significant downside of the $Li_4Ti_5O_{12}/LiFePO_4$ pair is their poor conductivity. As such they cannot be used in their bulk form in any realistic Li-ion batteries. However, as discussed above reduction of the particle size to the nanoscale can help overcome this issue (Kavan et al., 2003). As the primary particle size decreases 1) the diffusion path

length within the particles decreases and 2) the surface area of the electrode in contact with the electrolyte increases. These lead to lowered resistance to the intercalation reactions.

On the other hand, the conductivity of the material can be increased using conductive doping. For example silver (Huang et al., 2007) or copper (Wang et al., 2009) doping have been found to increase the electrochemical performance of LTO by about 20 and 50%, respectively. Also carbon coating has been used to coat LFP particles (Waser et al., 2011) leading to improvement of about 20% in the specific capacity.

Both the reduction in the primary particle size and the conductive doping can be can be achieved using aerosol based synthesis processes. As such they provide ideal methods for the synthesis of advanced materials for the next generation of Li-ion batteries.

3 Experimental methods

In this work two gas-phase techniques for synthesis of nanoparticles from liquid precursor solutions were utilised: Spray Pyrolysis and Flame Spray Pyrolysis. Table 3 lists the materials produced in the Papers I-IV along with methods and precursors used, and the analyses carried out.

3.1 Synthesis techniques

The various aerosol based nanoparticle formation routes have been outlined previously by, for example, Gurav et al. (1993); Pratsinis (1998, 2010); Mäkelä et al. (2004); Strobel and Pratsinis (2007). Figure 3 collates and extends those outlines to show a schematic of the various paths aerosol-based, high-temperature nanoparticle synthesis processes are likely to follow.

3.1.1 Spray pyrolysis

Spray pyrolysis (SP, Figure 4) was used in Paper I (Figure 1) to synthesise Gold nanoparticles from a organometallic complex precursor, as well as in Paper II (Figure 1) for the production of $LiFePO_4$ nanoparticles from low-cost alternative precursors.

The precursor solution was aerosolised, using a constant output atomiser (TSI Inc 3076, Paper I) an ultrasonic nebuliser (RBI Pyrosol 7901, Paper II), and the produced droplets carried into the reactor with a carrier gas. The reaction conditions were controlled through the choice of the carrier gas, the reactor temperature, and the residence time.

The aerosol exiting the heated zone was rapidly cooled with a large volume of dilution gas. This reduced the aerosol concentration and halted the sintering of the particles limiting the primary particle growth and the degree of agglomeration. in addition, the chemical reactions terminated allowing formation of metastable phases.

Table 3: List of synthesised materials and the methods used.

Product	Method	Application	Precursors	Analyses	Reference
Nano gold	SP	Optical, catalytic biomedical	$AuC_{11}H_{20}O$	SMPS, Gas FTIR, XRD, Raman, TEM	Paper I
$LiFePO_4$	SP	Li-ion battery, super capacitor	$LiOH \cdot H_2O$, H_3PO_4, $FeSO_4 \cdot 7\,H_2O$,	XRD, TEM	Paper II
$Li_4Ti_5O_{12}$	FSP	Li-ion battery, super capacitor	$C_5H_7LiO_2$, $C_{12}H_{28}O_4Ti$, $C_8H_{15}AgO_2$, $C_{16}H_{30}CuO_4$	CPC, FMPS, XRD, TEM, BET, Electrochemical	Papers III and IV

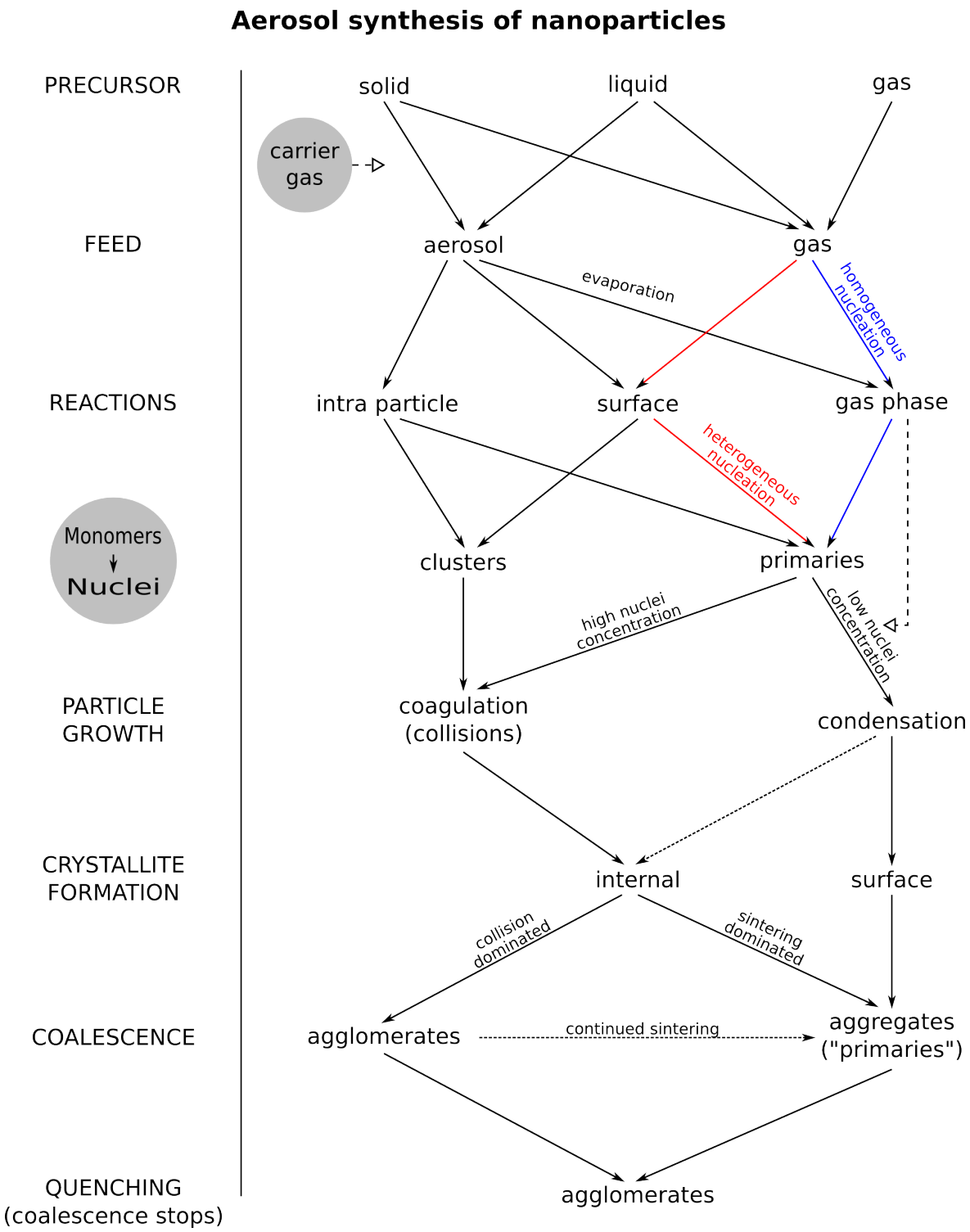

Figure 3: Outline of nanoparticle formation routes in high-temperature gas-phase synthesis.

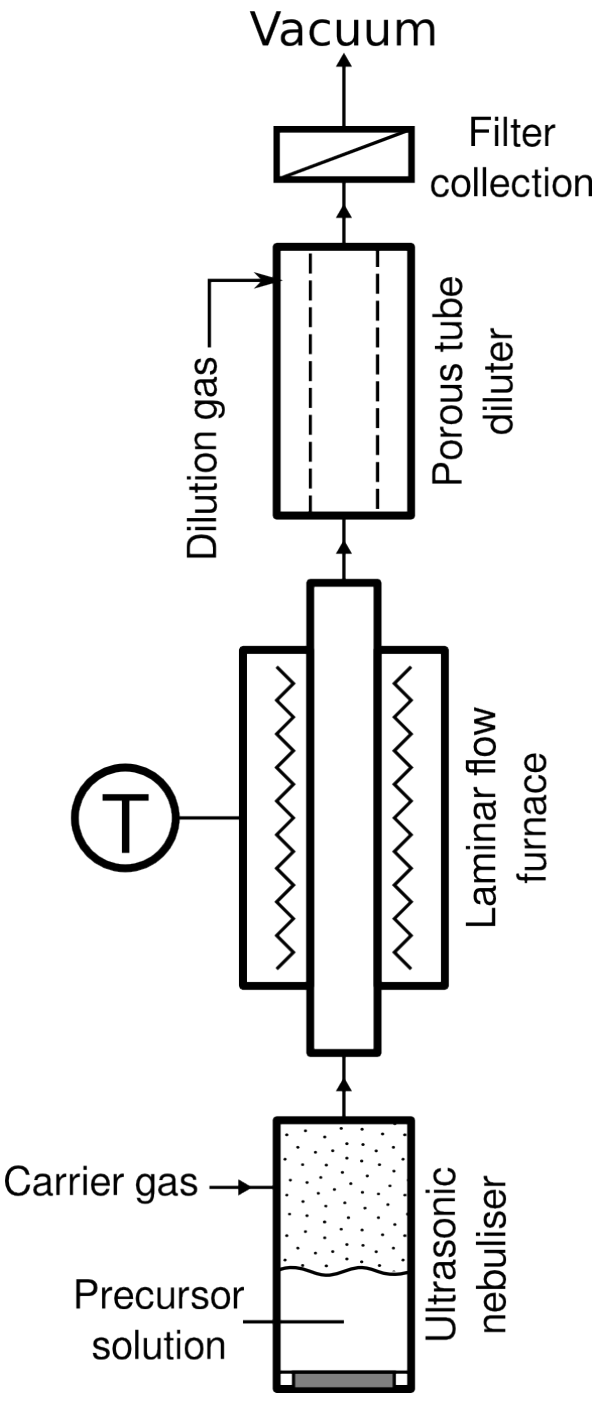

Figure 4: Schematic of the spray pyrolysis reactor used to to synthesise $LiFePO_4$ nanoparticles. (Published in Paper II)

3.1.2 Flame spray pyrolysis

Flame Spray Pyrolysis (FSP, Figure 5) was utilised in Paper III (Figures 1-2) for synthesis of single-crystalline $Li_4Ti_5O_{12}$ nanoparticles. In this standard FSP process the quenching of the particle sintering is very efficient (Ströbel and Pratsinis, 2007). As such primary particle size remains small (about 10 nm). However, it also stops the growth and ordering of the crystallite structures leading to poor Li-intercalation performance (cf. Section 4.2.1).

In Paper IV (Figure 1) the system was modified to extend the high-temperature residence time and thus encourage crystalline growth. This was achieved by directing the exhaust from the flame through a laminar flow reactor placed above the FSP. The quenching was, then, done downstream of the reactor. The aerosol temperature remained above 500 °C for about 1 s, compared to the residence time within the flame of about 1 ms in the standard set-up. This control of the high-temperature residence time allowed for the primary particle size to be tuned, and better crystallisation to be achieved.

3.2 Analysis techniques

In order to effectively determine the properties of the synthesised nanoparticles a number of online and offline techniques need to be employed. In this work the properties of the particle agglomerates produced were analysed using online aerosol analysis instruments (3.2.1). The reactions taking place in the synthesis were, furthermore, monitored by analysing the gaseous compounds downstream of the reactor (3.2.2).

The chemical and crystalline properties of the synthesised particles were analysed with X-ray techniques (3.2.3) or spectroscopic techniques (3.2.4). While the morphology of the primary particles were determined with electron microscopy (3.2.5) and nitrogen adsorption (3.2.6).

Lastly, the suitability of the material for Li-ion battery applications were tested via electrochemical cycling of Li-ion half cells (3.2.7).

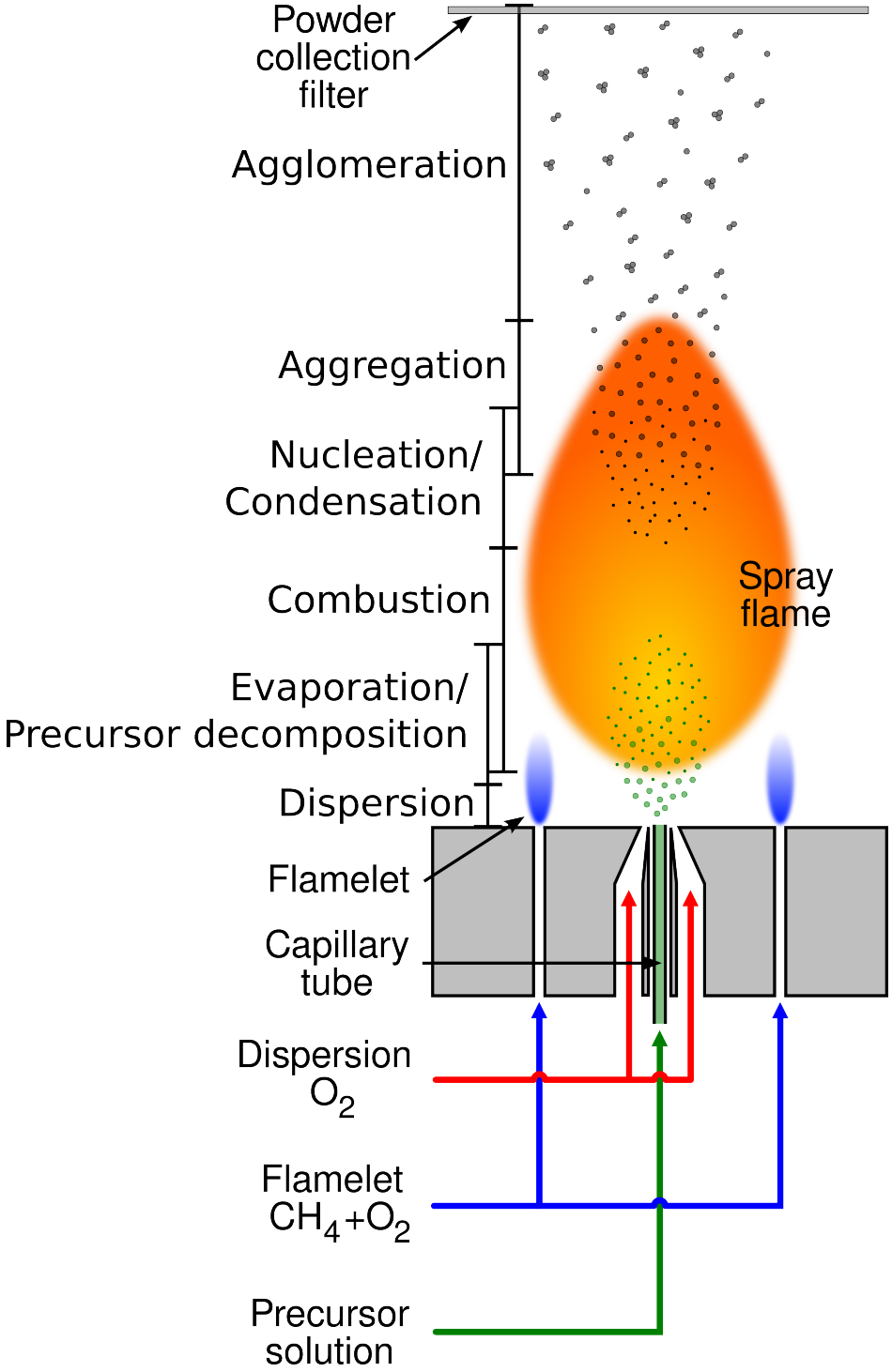

Figure 5: Schematics of the flame spray pyrolysis reactor used to synthesise $Li_4Ti_5O_{12}$ nanoparticles. (Published in Paper III)

3.2.1 Aerosol properties

In Paper I and Paper III the physical characteristics of the nanoparticle agglomerates were measured directly from the aerosol flow leaving the respective reactors. The diluted samples were analysed online using a condensation particle counter (CPC, TSI CPC 3775), a scanning mobility particle sizer (SMPS, TSI DMA 3081 + CPC 3776) or a fast mobility particle sizer (FMPS, TSI FMPS 3091).

The CPC provides high time-resolution measurement of the total particle number concentration and is thus ideal for monitoring temporal variations in the synthesis process. The SMPS and FMPS, on the other hand, measure the electrical mobility size distribution of the synthesised particles. SMPS has a high size resolution but takes a few minutes to complete a scan, while FMPS has fewer size bins but can scan the entire size range in seconds. In this work both will provide information about the agglomerates formed during the synthesis before further agglomeration in powder collection.

3.2.2 Gas monitoring

In Paper I gaseous compounds remaining after or produced during the particle synthesis were characterised online using a fourier transform infrared spectroscope (FTIR, Temet Instruments GASMET DX-499). This method provides gas composition by measuring the infrared absorption spectrum of the gas and comparing it to the characteristic spectra for various reference compounds.

3.2.3 X-ray techniques

X-ray diffraction (XRD) technique was used in all the papers (I-IV) as it is a powerful method for providing chemical and crystallographic information for a bulk sample. In Papers I, II and IV the analysis was performed on a Bruker D8 Discover (Cu Kα source, 40 kV, 40 mA) and analysed with the Topas 3 software; while in Paper III a Bruker D8 AXS D8 Advance was used. In both Cu Kα source was used (40 kV, 40 mA).

The diffraction was generally measured between 2θ angles of 10 and 90° with step size of 0.06° or less. The crystallite sizes, d_{XRD}, were calculated based on the fundamental parameter approach and the Rietveld method. The compounds present were detected

by using the ICSD crystallographic database and abundances estimated using whole diffractogram fitting with Topas 3 software.

Furthermore, in Paper III the elemental purity of the samples was determined with X-ray fluorescence (XRF) using a Philips PW2404 X-ray spectrometer. From this a semi-quantitative elemental analysis was obtained using the SemiQ program. Powder collected on a PTFE fibrous filter was used for both techniques; samples down to a few milligrams can be analysed.

3.2.4 Raman spectroscopy

In addition to the X-ray techniques Raman spectroscopy was used in Paper I to identify amorphous compounds present in the samples. A Bruker Senterra 200 LX Raman was used to record the Raman spectra which was then compared to reported peak positions for Raman scattering by carbon. Only a few crystals of the product powder, collected on a PTFE fibrous filter, was needed for the analysis.

3.2.5 Electron microscopy

The size and structure of the synthesised nanoparticles were imaged directly using field emission transmission electron microscope (TEM). In papers I, II and IV the imaging was carried out with a JEM-2100F (JEOL Ltd.), while for paper III a Philips CM-200 (FEI company) was used.

Bright and dark field (BF/DF) imaging, selected area diffractometry (SAED), high angle annular dark field scanning TEM (HAADF-STEM) and energy dispersive X-ray spectrometry (EDS) were performed. In Papers I and II a point-to-plate electrostatic precipitator (ESP, InTox Products) was used to obtain the particle samples directly from the aerosol stream on to a holey carbon copper grid (Agar Scientific Ltd.). In Papers III and IV to prepare the samples the collected powders were first dispersed into ethanol. An electron microscope sample grid (Agar Scientific), with perforated amorphous carbon supported on a copper mesh was then dipped into the dispersion and allowed to dry in room temperature before the imaging.

3.2.6 Nitrogen adsorption

While the TEM imaging provides the sizes of individual primary particles and the XRD the crystallite size for the bulk sample these do not necessarily correspond to the average primary particle size for the bulk sample. To determine this a nitrogen adsorption technique (BET) first reported by Brunaer, Emmett and Teller (Brunauer et al., 1938) was used in Paper III.

The samples of collected powder were first dried at 150 °C for at least one hour at atmospheric pressure to remove the adsorbed water. Then a five-point nitrogen adsorption isotherm at 77 K was measured using Tristar gas adsorption instrument (Micrometrics Instruments Corp.) and the specific surface area (SSA) determined. From this the primary particle size can be calculated using (2) (with a bulk density ρ).

$$d_{\mathrm{BET}} = \frac{6}{\rho \times SSA} \tag{2}$$

3.2.7 Electrochemistry

The electrochemical performance of the materials were tested using a multi channel battery tester (Maccor Inc.). The collected product powder was first sieved (45 µm cut-off) and dried overnight. An electrode slurry containing the active material (80 m-%), PVDF (Kureha #1100, 10%), and conductive carbon (Timcal C65, 10%) was prepared and doctor bladed (150 µm, 100 m/s) onto an Al-foil (20 µm). The foil was then dried overnight at 120 °C in vacuum, and pressed in a calender.

Electrodes (14 mm diameter) were cut from the sheets and assembled into half-cells (CR 2016 type) with a lithium counter electrode and a glass fibre separator. The chosen electrolyte was $LiPF_6$ in EC:DMC:DEC. These cells were then cycled between 1 and 3 V through a program of several constant current charge-discharge sequences. The current rates were chosen to correspond to the C-rates of 0.2, 0.5, 1, 2, 5, and 10. The resulting capacities were scaled with the active material mass to obtain specific capacity values for each C-rate.

The C-rate has units of h^{-1} and is defined by (3), where q is the theoretical maximum specific capacity of the electrode material under study (mAh/g), i is the specific

charge/discharge current used (mA/g), and τ is the time taken to fully charge/discharge the cell (h).

$$\text{C-rate} = \frac{1}{\tau} = \frac{i}{q} \tag{3}$$

4 Results and discussion

4.1 Nanoparticle formation in high-temperature conditions

In this study engineered nanoparticles have been produced using two high-temperature synthesis methods: Spray Pyrolysis (3.1.1) and Flame Spray Pyrolysis (Section 3.1.2). Both methods enable control of the synthesis conditions and, thus, tuning of the product properties. Figure 6 shows the likely paths taken by the particle formations in the current experiments. The start and end conditions, liquid precursor solutions and nanoparticle agglomerates, respectively, are known while the intermediate steps are assumed.

4.1.1 Gold nanoparticles

For the spray pyrolysis processes in paper I and II the feed into the reaction zone is in the form of aerosol composed of precursor solution droplets and carrier gas. From here on the path likely follows mainly left-hand side of the schematic with reactions taking place within or on the surface of the evaporating droplets, and the crystallites forming in the solution. The end product properties could thus be controlled by varying the precursor stoichiometry, solvent chemistry and the droplet heating rate.

For the flame pyrolysis used in papers III and IV the precursor solution is also aerosolised. However, the temperatures involved result in very rapid evaporation of the precursor and solvent. Thus, the path will follow mostly the right-hand side of the schematic: the reactions take place in the gas phase. Also since the produced powders always seem to be composed of single-crystalline primary particles it is likely that either 1) the crystallites form by growth of the nuclei through condensation, 2) or the coalescence is sintering dominated until the quenching takes place.

Paper I describes a process for the synthesis of gold nanoparticles (AuNPs) using an atmospheric-pressure, aerosol-assisted technique. The gold precursor was a homoleptic cluster $(AuC_2R)_{10}$ (R = 2,6-dimethyl-4-heptanol) designed to be stable in air (Koshevoy et al, 2012) and dissolved into either ethanol or hexane.

The synthesis technique was based on spray-pyrolysis within a heated laminar flow furnace. The precursor solution was aerosolised and carried with a flow of nitrogen

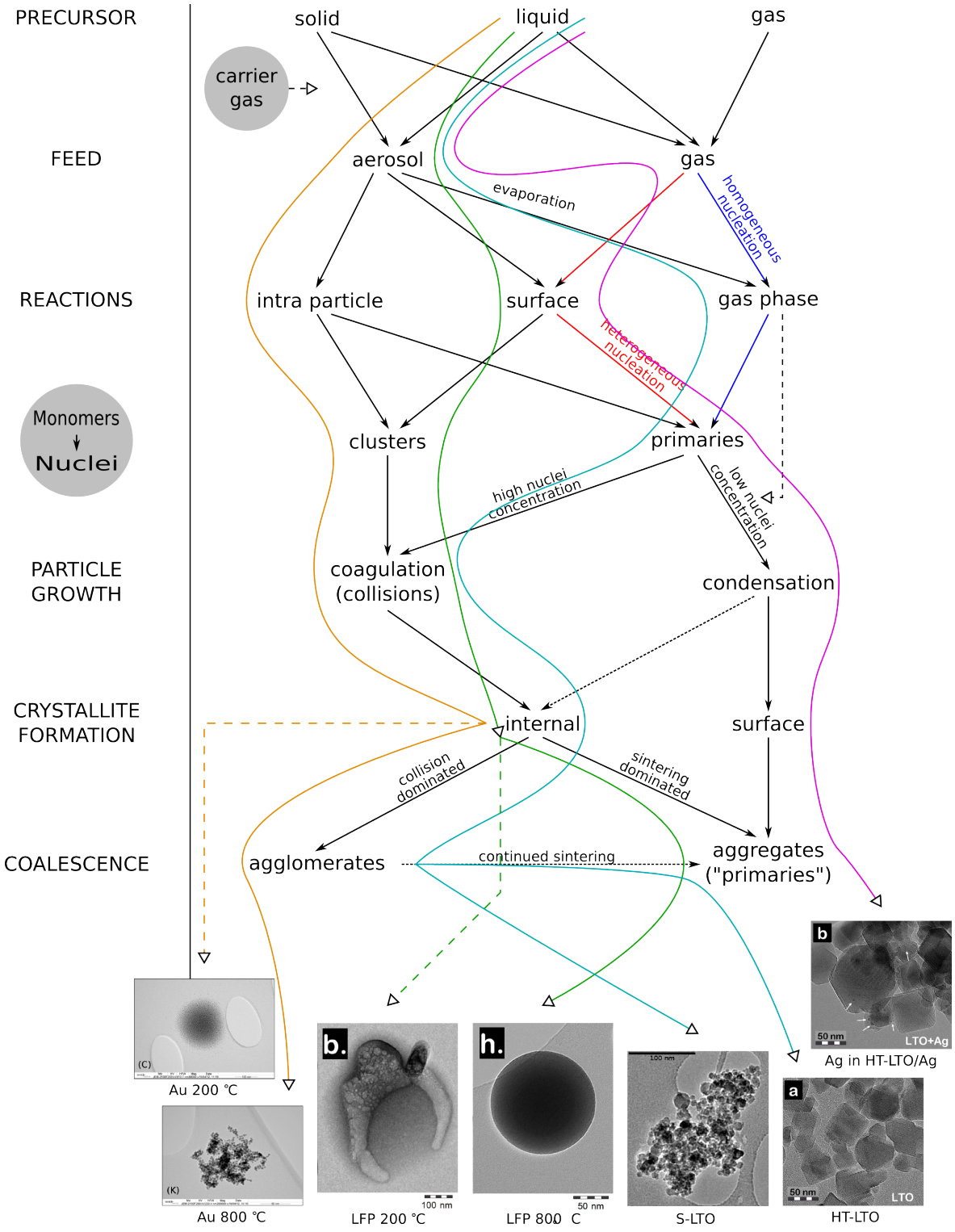

Figure 6: The assumed particle formation routes realised for gold (Paper I), $LiFePO_4$ (Paper II), and $Li_4Ti_5O_{12}$ (Paper III and IV) nanoparticles.

into the heated furnace. Here the aerosol droplets underwent rapid evaporation and acted like microreactors in which a large number of monodisperse, nanosized, non-sintered AuNPs formed within the span of a few seconds.

The particle size, crystallinity, structure, and surface morphology of the product powders were analysed using a number of instruments. This allowed for a investigation into the effects of the process condition (solvent, atmosphere and temperature) on the product properties to be carried out.

The temperature of the synthesis was found to have major impact on the product. A dramatic change of colour from bright yellow to very dark red was observed as the temperature of the furnace was increased from 200 to 800 °C (Figures 7A, E, I).

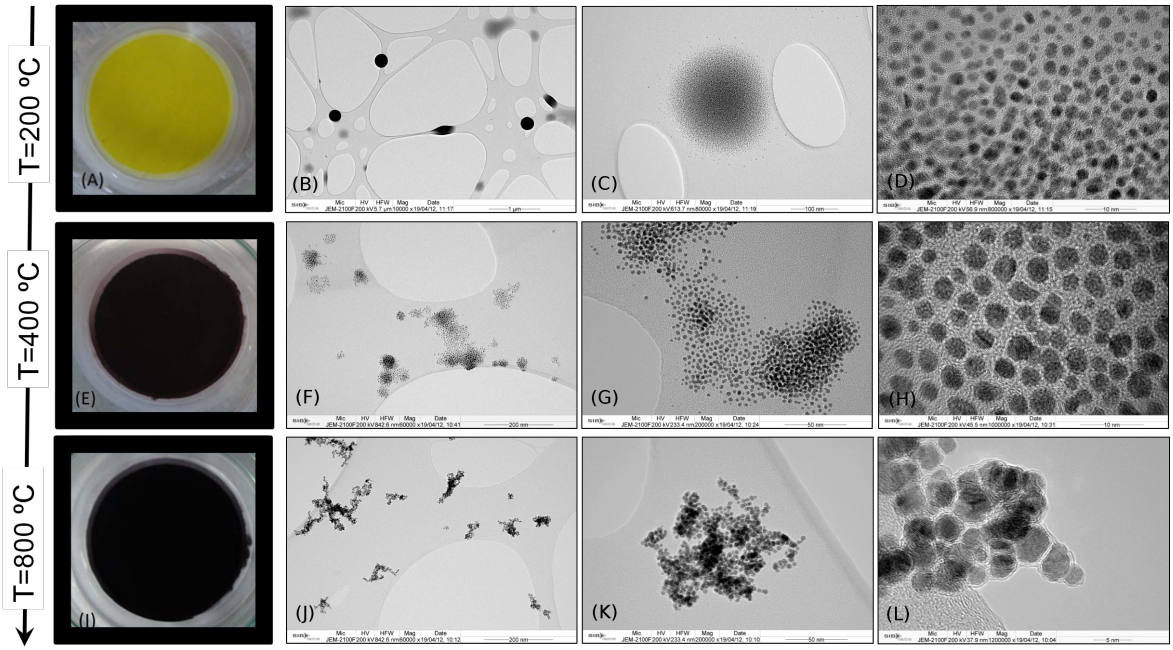

Figure 7: Gold nanoparticles synthesised via a spray pyrolysis route at various temperatures. Photographs of filters with collected powders (left column) and TEM micrographs of the particles at several magnification factors. (Published in Paper I)

At the same time a clear transformation from droplet-like, spherical gold particle clusters to solid, irregular nanoclusters took place (Figures 7B-C, F-G, J-K). The primary particle size was found to be below 5 nm in all cases with no significant sintering taking place even at high synthesis temperatures (Figures 7D, H, L).

Furthermore, XRD data (Figure 8) showed that the produced crystallites were phase

pure gold for all process conditions, with the exception of the synthesis at 200 °C where X-ray amorphous powder was produced. The crystallite sizes increased slightly as temperature was increased from 400 to 800 °C, ranging from 2.3 to 2.8 nm for ethanol and from 1.8 to 2.3 nm for hexane solvent.

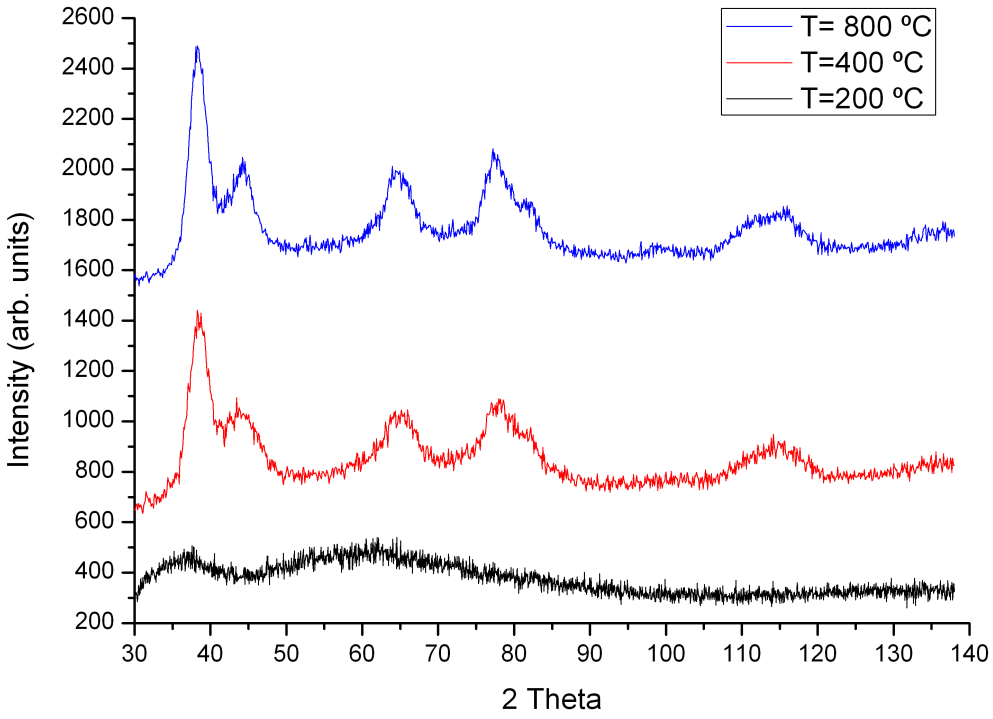

Figure 8: X-ray diffractograms of gold nanoparticles synthesised via a spray pyrolysis route at various temperatures. (Published in Paper I)

When ethanol was used as the solvent the gas FTIR data downstream of the furnace showed presence of ethanol oxidation products (e.g. acetaldehyde). These longer chained hydrocarbons were found not to evaporate completely at 200 °C leading to droplet-like particles.

However, as the temperature was increased further decomposition of the ethanol or these other hydrocarbons was found to form a carbon layer onto the gold nanoparticles. This was observed in the Raman (Figure 9) spectra as an increase in the carbon D and G band signals.

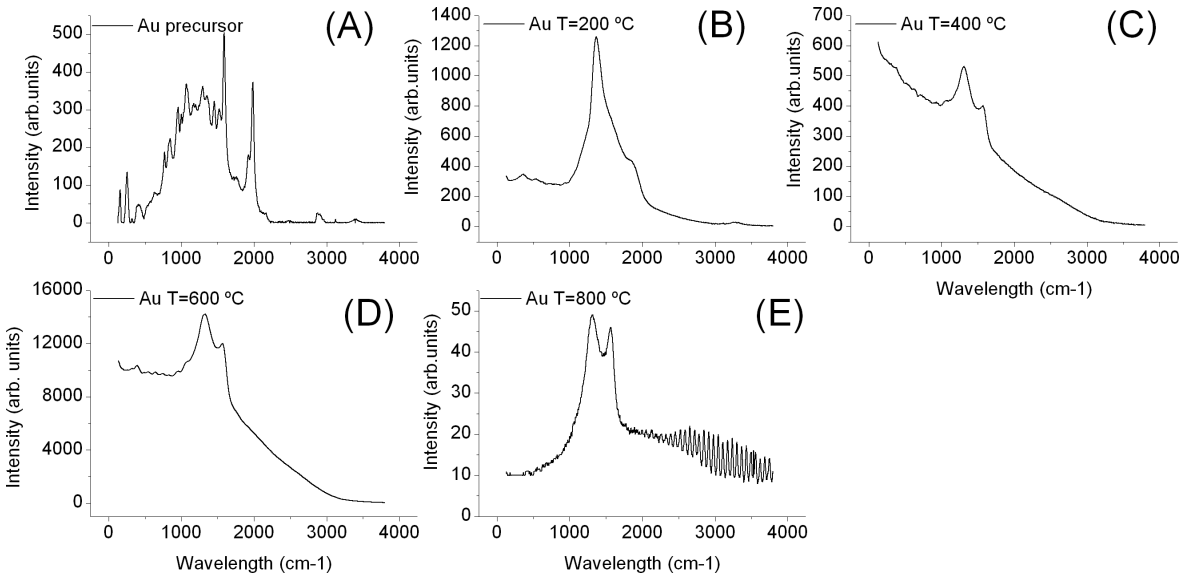

Figure 9: Raman spectra of gold nanoparticles synthesised via a spray pyrolysis route at various temperatures. (Published in Paper I)

4.1.2 $LiFePO_4$ nanoparticles

Aerosol-assisted synthesis of $LiFePO_4$ nanoparticles was carried out using $FeSO_4 \cdot 7\,H_2O$ produced as by-product of industrial processing. The iron sulphate was mixed with LiOH and H_3PO_4 in a simple aqueous solution and aerosolised with an ultrasonic nebuliser. When the resulting droplets were heated to 800 °C in laminar flow reactor a powder composed mainly of LFP was obtained.

It was found that the formation of $LiFePO_4$ requires sufficiently long residence time in the high-temperature reaction zone after the solvent has evaporated. In the current set-up, this condition was fulfilled by a carrier gas flow of 1.5 L/min and reactor temperature of 800 °C. Figure 10 shows the XRD data for products synthesised at various temperatures. At temperatures below 800 °C there exists significant amounts of compounds other than $LiFePO_4$, mainly lithium and iron sulphates and phosphates.

Figure 11 shows the TEM images of the synthesised particles. From this it can also be seen that at low temperatures the particles were droplet-like containing smaller salt crystals indicating incomplete evaporation of the solvent. At 800 °C, however, the solvent evaporated more rapidly. Thus the dry particle had sufficient residence time at the high-temperatures to produce solid and homogeneous $LiFePO_4$ particles.

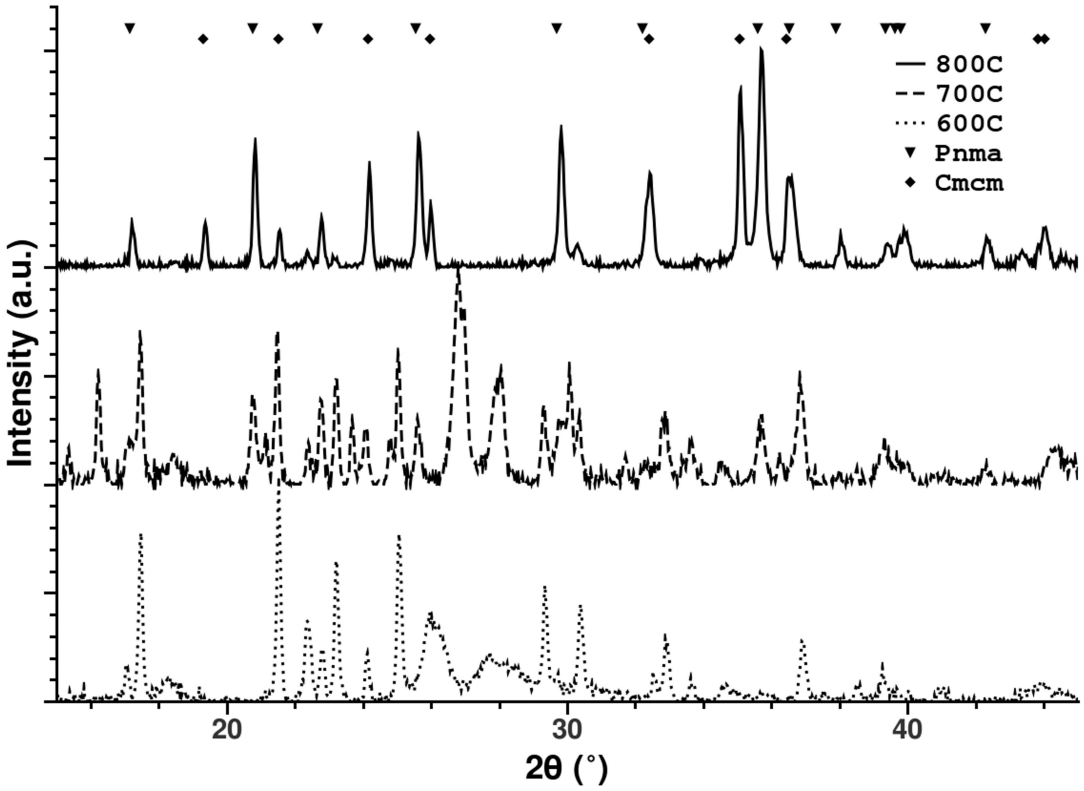

Figure 10: X-ray diffractograms of $LiFePO_4$ synthesised via spray drying at various temperatures. (Published in Paper II)

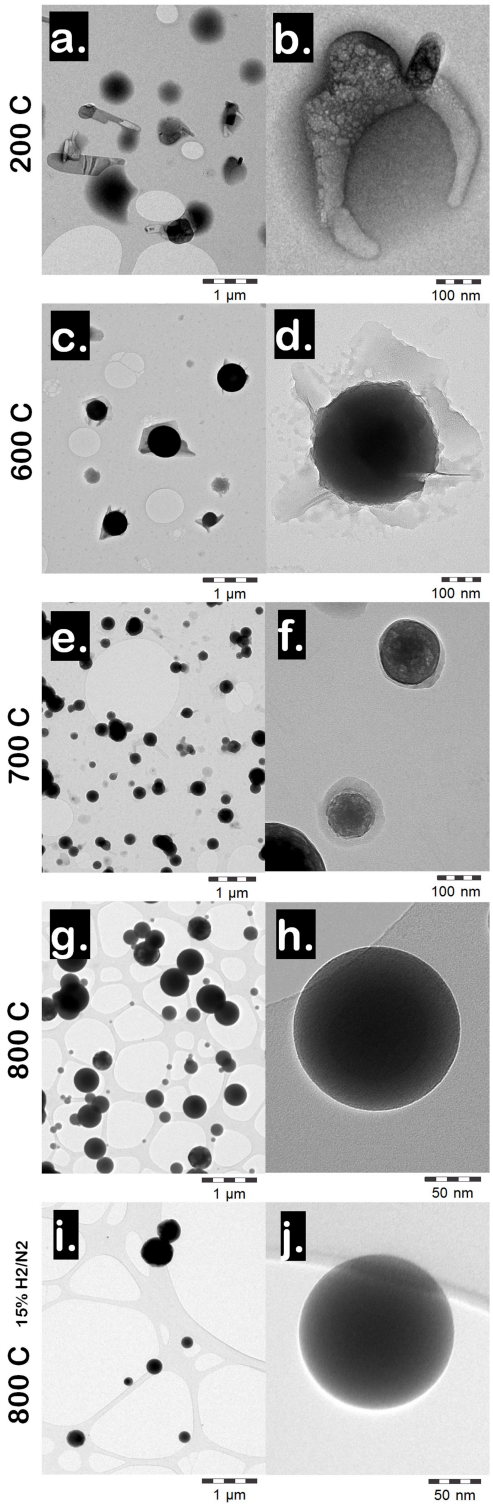

Figure 11: TEM micrographs of $LiFePO_4$ synthesised via spray drying at various temperatures. (Published in Paper II)

The chemical reactions taking place can be fine tuned by altering the reducing potential of the reaction environment and the stoichiometry of the precursor solution. Introducing hydrogen into the carrier gas resulted in increased fraction of the olivine polymorph of $LiFePO_4$ but also led to increased abundance of impurities (mainly Li_3PO_4) (Figure 12).

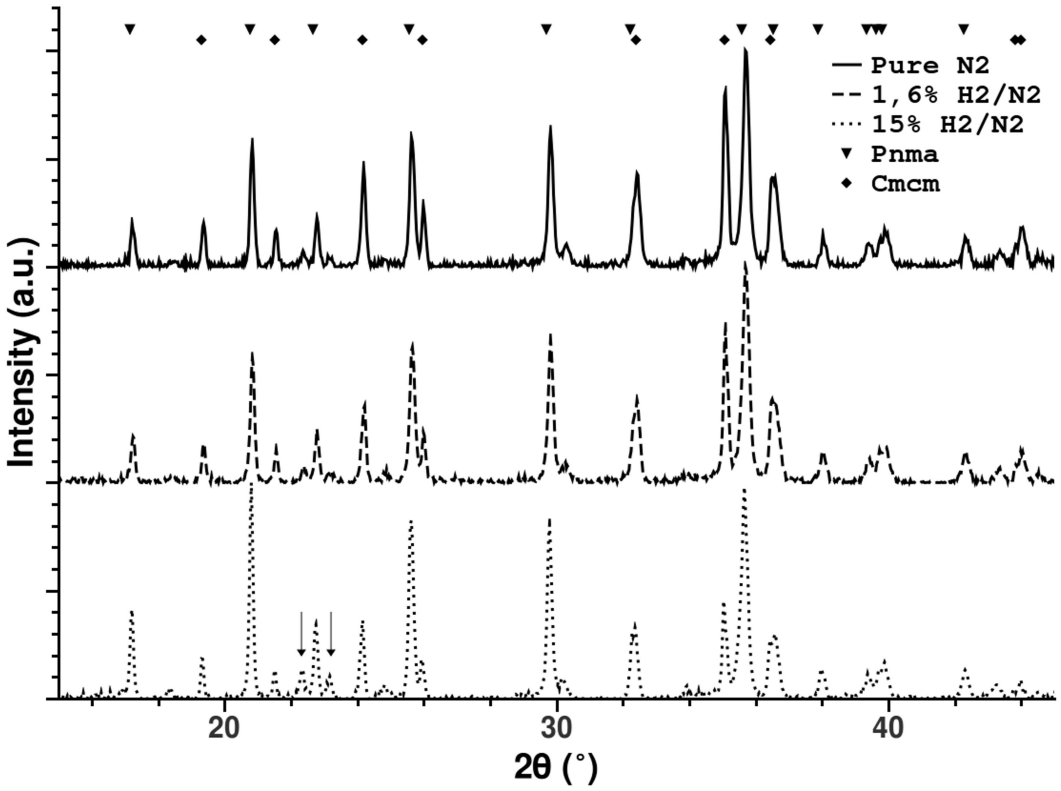

Figure 12: X-ray diffractograms of $LiFePO_4$ synthesised via spray drying at various reaction atmospheres. (Published in Paper II)

Unlike for hydrothermal synthesis of LFP (Qin et al., 2010) for the aerosol synthesis excess Li stoichiometry will also result in Li_3PO_4 impurities. Conversely, increasing the iron content of the precursor solution resulted in higher fraction of the high-pressure polymorph of LFP but also promoted formation of electrically conductive impurities (e.g. Fe_2O_3) (Figure 13).

The optimum choice of the reaction atmosphere and precursor stoichiometry depends on the requirements of the application. The olivine LFP is known to have higher specific capacity than the high-pressure polymorph. On the other hand, increasing abundance

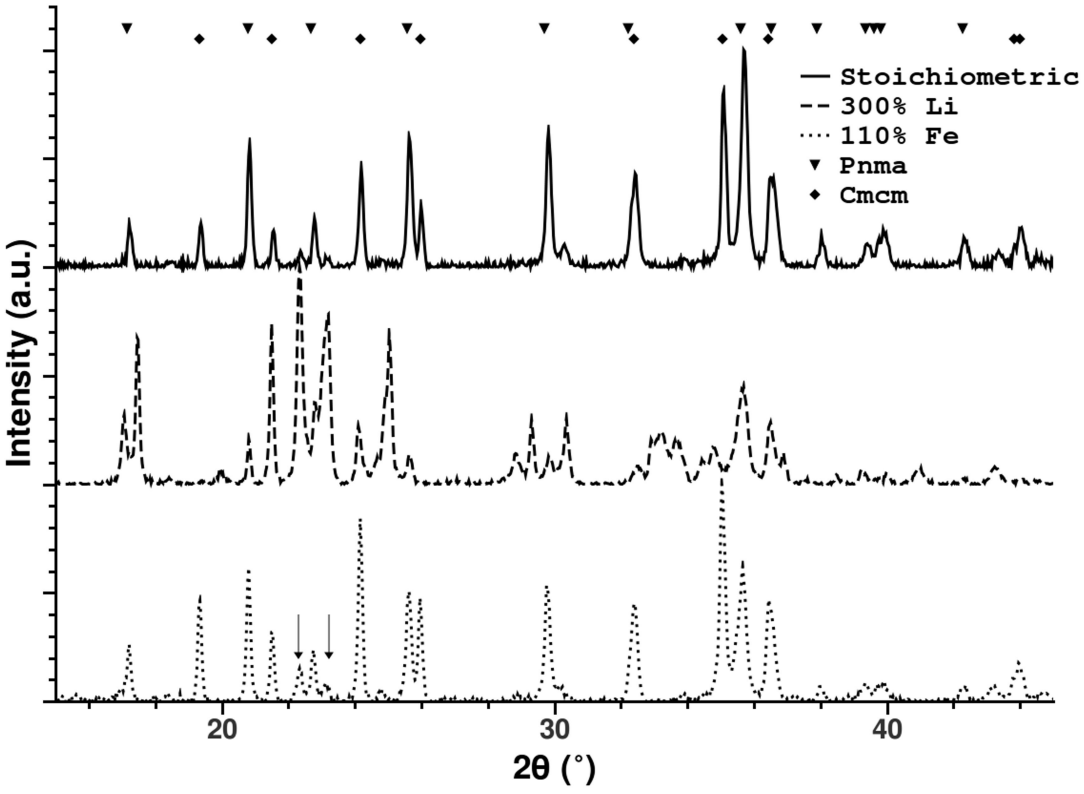

Figure 13: X-ray diffractograms of $LiFePO_4$ synthesised via spray drying with various precursor stoichiometries. (Published in Paper II)

of Li_3PO_4 and Fe_2O_3 are likely to decrease and increase the electrical conductivity of the material, respectively.

Thus, for a high capacity battery applications, the optimum product composition will likely be obtained in inert atmosphere with stoichiometric precursor concentrations. For high power applications, on the other hand, the optimum set-up would probably be reducing atmosphere with iron excess, or lithium deficiency. This should promote the formation of electrically conductive iron oxides and phosphates and to reduce the abundance of poorly conductive Li_3PO_4.

4.1.3 $Li_4Ti_5O_{12}$ nanoparticles

Paper III describes a gas-phase technique for simultaneous synthesis and doping of $Li_4Ti_5O_{12}$ nanoparticles (Figure 5). The flame spray synthesis (FSP) process was found to be fast and steady as illustrated by the number concentration time series in Figure 14 and the agglomerate size distributions shown in Figure 15.

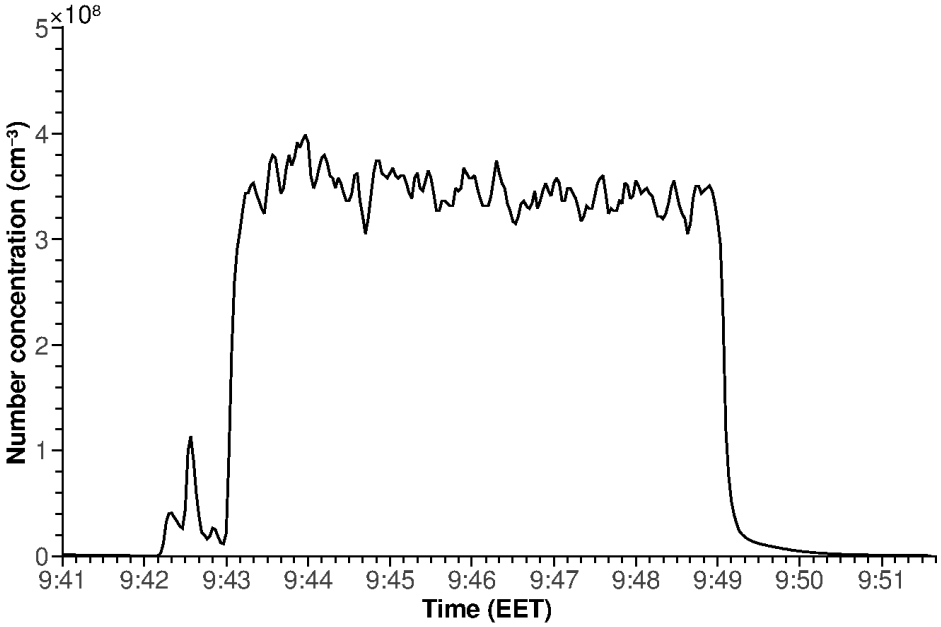

Figure 14: Time evolution of the particle number concentration during synthesis of $Li_4Ti_5O_{12}$ via a flame spray pyrolysis route. (Published in Paper III)

The resulting particles were found to have a high elemental purity ($> 99\%$); and both primary (from BET) and crystallite (from XRD) sizes of about 10 nm, indicating single-

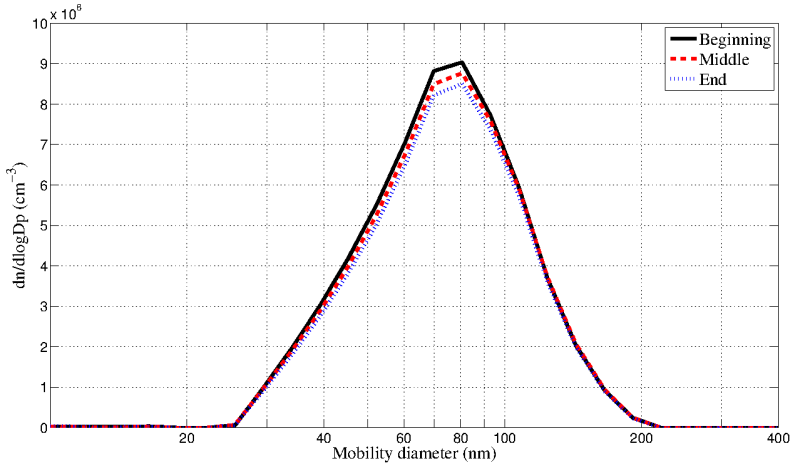

Figure 15: Size distribution of the particle number concentration during synthesis of $Li_4Ti_5O_{12}$ via a flame spray pyrolysis route. (Published in Paper III)

crystallite primaries. Formation of dense agglomerates with hundreds of these primary particles was observed in the gas phase (Figure 16) with further loose agglomeration during the powder collection. X-ray diffraction data (black line in Figure 17) also show that the undoped particles were phase pure $Li_4Ti_5O_{12}$.

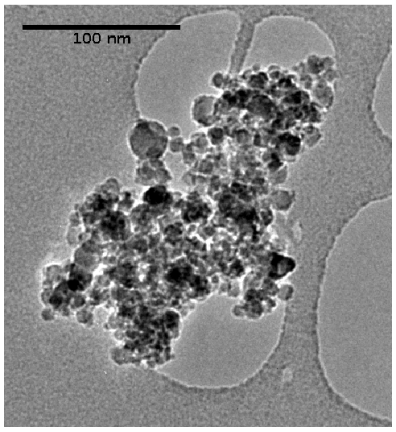

Figure 16: TEM micrograph of a sample agglomerate formed during synthesis of $Li_4Ti_5O_{12}$ via a flame spray pyrolysis route. (Published in Paper III)

However, as $Li_4Ti_5O_{12}$ has a poor electrical conductivity doping with both silver and copper was studied. The two dopants were found to behave very differently. The silver formed a separate phase of metallic silver with particle size of only a few nanometres, seen in Figure 17 at high dopant concentrations. This silver was seen to deposit on and

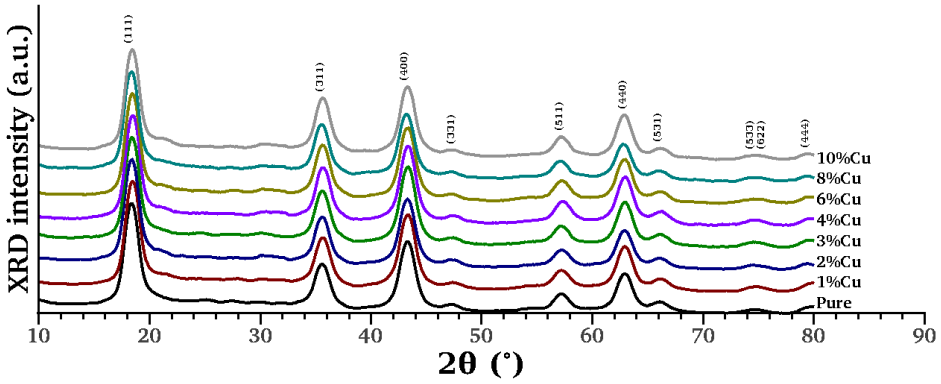

Figure 17: X-ray diffractograms of copper doped $Li_4Ti_5O_{12}$ synthesised via a flame spray pyrolysis route. (Published in Paper III)

between the LTO particles, leading to an LTO/Ag composite material (Figure 18b).

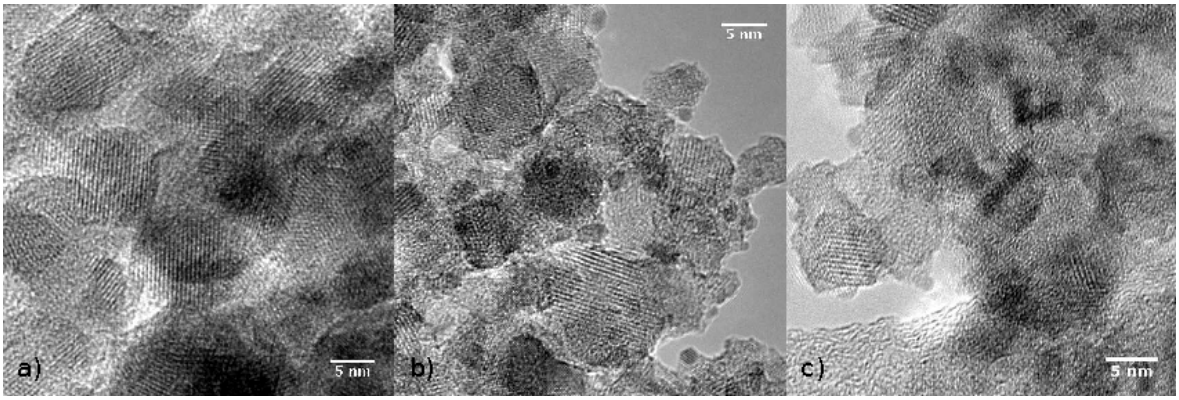

Figure 18: TEM micrographs of pure and doped $Li_4Ti_5O_{12}$ synthesised via traditional flame spray pyrolysis route. (Published in Paper III)

The copper, on the other hand, was found to react with the LTO to form a homogeneous $Li_4Ti_5O_{12}/Li_2CuTi_3O_8$ double spinel structure (Figure 18c). No additional peak were observed in the XRD data (Figure 19). Instead a change in the relative intensities of the (311) and (400) peaks of the $Li_4Ti_5O_{12}$with increasing copper content was found. This is a result of the substitution of Li and Ti atoms by copper within the spinel structure.

When these FSP synthesised $Li_4Ti_5O_{12}$ particles were used in Li-ion test cells it became apparent that their performance fell short of the expected. Based on literature it seemed likely that this was a result of the extremely small crystallite size (10 nm) of the particles (cf. Section 4.2.1).

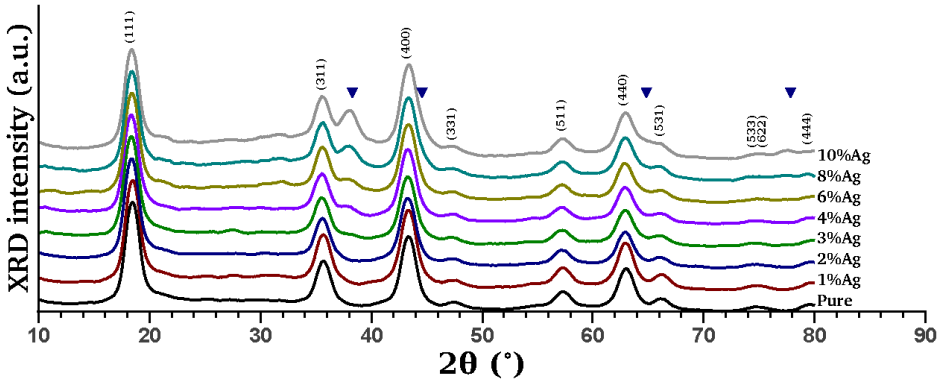

Figure 19: X-ray diffractograms of copper doped $Li_4Ti_5O_{12}$ synthesised via a flame spray pyrolysis route. (Published in Paper III)

To overcome this performance limitation in Paper IV a modified FSP system was designed to encourage growth of the crystallites. This was achieved by adding a vertical flow furnace into which the combustion gases from the FSP flame were drawn. The furnace was maintained at 1000 °C to extend the high-temperature residence time of the nanoparticles.

This extended high-temperature residence was found to increase the primary particle and crystallite sizes from 10 nm to about 40 nm. Furthermore, the particle morphology became more faceted indicating more crystalline structure, as seen in Figure 20a.

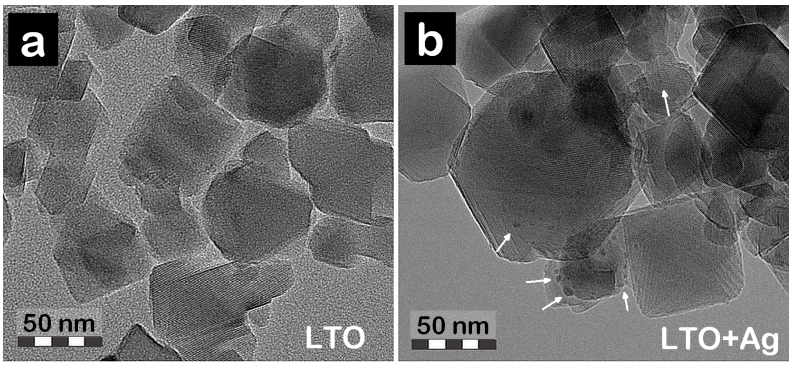

Figure 20: TEM micrographs of pure and doped $Li_4Ti_5O_{12}$ synthesised via high-temperature flame spray pyrolysis route. (Published in Paper IV)

However, the modification did not seem to have significant effects on the behaviour of the silver dopant. A few nanometre sized metallic silver particles were still found on the surface of the $Li_4Ti_5O_{12}$ particles as illustrated by the HAADF images and

corresponding EDS spectra in Figure 21.

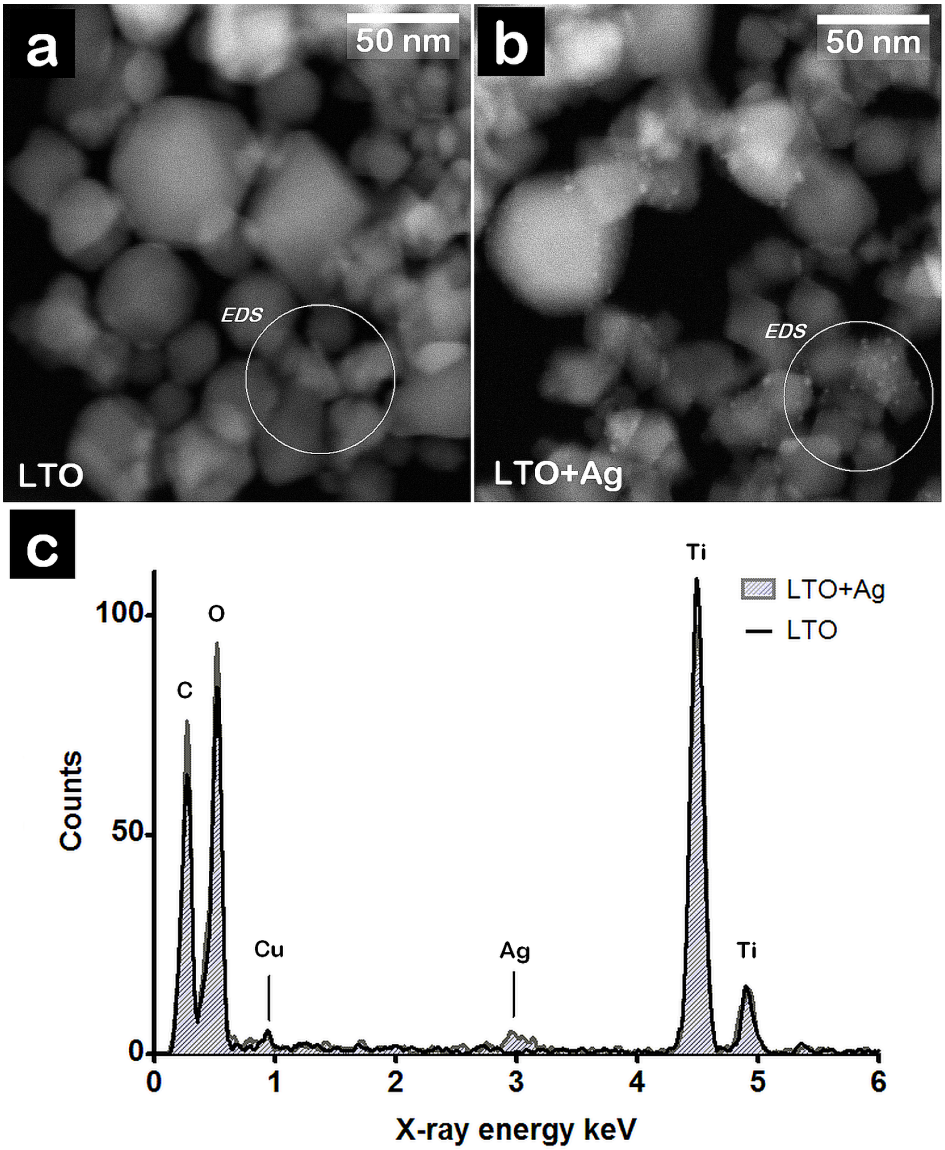

Figure 21: HAADF image of (a) pure and (b) Ag-doped $Li_4Ti_5O_{12}$ synthesised via high-temperature flame spray pyrolysis route. (c) EDS spectra for the regions indicated by the white circles in a and b. (Published in Paper IV)

The extension of the high-temperature residence time (1 ms to 1 s in Paper IV) encourages the growth of the crystallites and the primary particles. A vertical flow furnace added to the FSP system provides a convenient way to achieve this extension. It will also allow optimisation of the residence time and furnace temperature to achieve particles of the desired size.

4.2 Nanoparticles as electrode materials

4.2.1 Effect of crystallite size

As reported in Paper IV the crystallite size of $Li_4Ti_5O_{12}$ nanoparticles have a significant effect on the materials electrochemical behaviour. The high-temperature synthesis of LTO was found to increase the crystallite size form 10 nm to 40 nm. This resulted in a significantly improved specific capacity as illustrated in Figure 22.

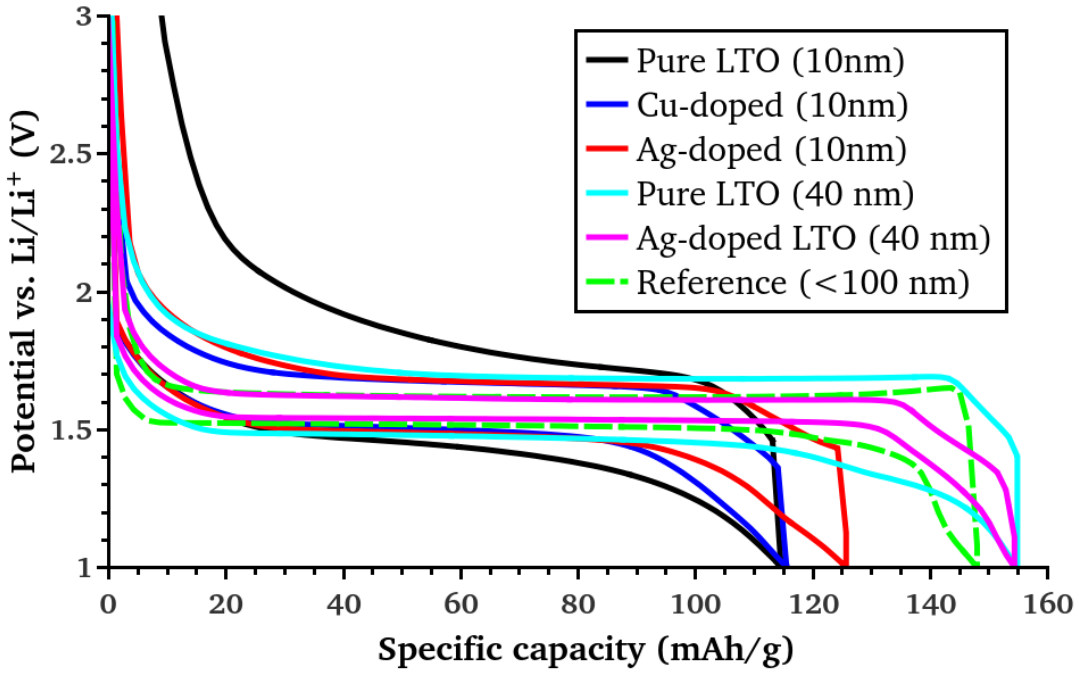

Figure 22: Capacity-voltage (CV) plots of Li-ion half-cells assembled using $Li_4Ti_5O_{12}$ as the negative electrode. The CV data was measured at rate of 1C and the dopant amount were 4% i each of the doped samples. (Based on the results presented in Paper IV)

This is consistent with a dependence of specific capacity with crystallite size reported by Kavan et al. (2003). They found an optimal crystallite size for $Li_4Ti_5O_{12}$ to be about 20 nm with the capacity falling rapidly for smaller sizes at all C-rates. This is a result of the reduction in the density of effective intercalation sites within the crystallite lattice of the electrode particles. The smaller the particle the higher the curvature at

the surface of the particle and, thus, the higher the fraction of the particle volume with distorted crystallite structure.

For larger crystallite sizes the reduction in the capacity was found to depend on the C-rate, falling off faster for higher currents. This can be understood by considering the movement of the lithium ions within the electrode during the charge/discharge of the cell. For a lithium ion to move from the electrolyte to a intercalation site within an electrode particle it needs to: 1) transfer from the electrolyte to the surface of the particle, 2) combine with an electrode, and 3) diffuse through the particle to the intercalation site (Figure 23).

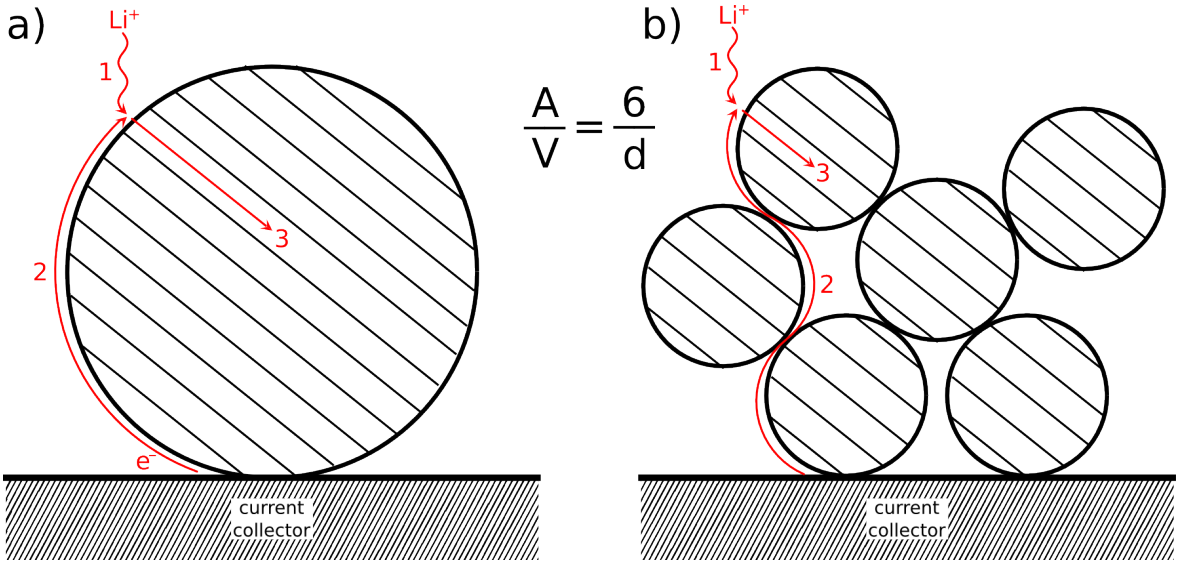

Figure 23: Schematic of diffusion paths at the negative electrode during cell charging.

The first step depends on the area of contact between the electrolyte and the electrode. As smaller primary particles result in higher specific surface area this charge transfer step is generally faster for smaller particles (Scrosati and Garche, 2010; Park et al., 2010).

The second step depends mainly on the availability of electrons. This can be a limiting step if the electronic contact between the reaction site and the current collector is compromised due to poor conductivity of the materials (for e.g. delithiated LTO) or disintegration of the electrode due to cycling (for e.g. Si) (Scrosati and Garche, 2010). To ensure proper electrical conduction a conductivity additive (e.g. conductive carbon) is generally mixed with the electrode material.

Lastly, the lithium diffusion speed within the particle is a property of the electrode material but can be compromised by crystalline defects (Park et al., 2010)). Furthermore, as the particle size decreases also the diffusion lengths within the particle, and thus the diffusion times, get shorter. Thus small single crystallite particles are optimal for the diffusion.

Now, at low current densities these Li-ion transfer rate limiting effects are not important and the capacity is simply proportional to the number of intercalation sites. On the other hand, at higher C-rates there might not be sufficient time for the intercalation to take place, especially deep within the electrode particles. Thus the capacity would fall of for larger primary particles, and the fall would be faster the higher the C-rate.

These effects can be visualised by considering a simple model of the lithium intercalation into the active material particle. Let us assume a spherical particle through which the intercalation proceeds at a constant rate from the surface inward. Furthermore, let us assume that near to the particle surface the intercalation is not fully effective, due to crystalline deformations or other surface effects, thus leaving a partially intercalated surface layer. A schematic of such a particle is shown as an inlay in Figure 24.

Now, using this model to calculate the effective utilisation factor at various C-rates for a range of particle sizes we can reproduce the main features of the variations of the specific capacity seen for the $Li_4Ti_5O_{12}$ nanoparticles. This theoretical utilisation is shown in Figure 24.

It can be readily seen that for low C-rates the particles can be very large and still achieve full utilisation. This results from the long charge cycle during which the intercalation can reach all the way to the core of the particle. At small particle sizes the relatively large volume fraction of the surface layer leads to a lower intercalation efficiency.

However, as the C-rate increases there is less time for the lithium to reach the intercalation sites in the particle core. Thus leaving a portion of the larger particles unutilised, while smaller particles are still fully utilised. The smallest particles still suffer from the inefficient utilisation of the surface leading to a optimal particle size for a given C-rate. This optimal size decreases as the C-rate increases; at the highest C-rates only the surface layer has time to intercalate.

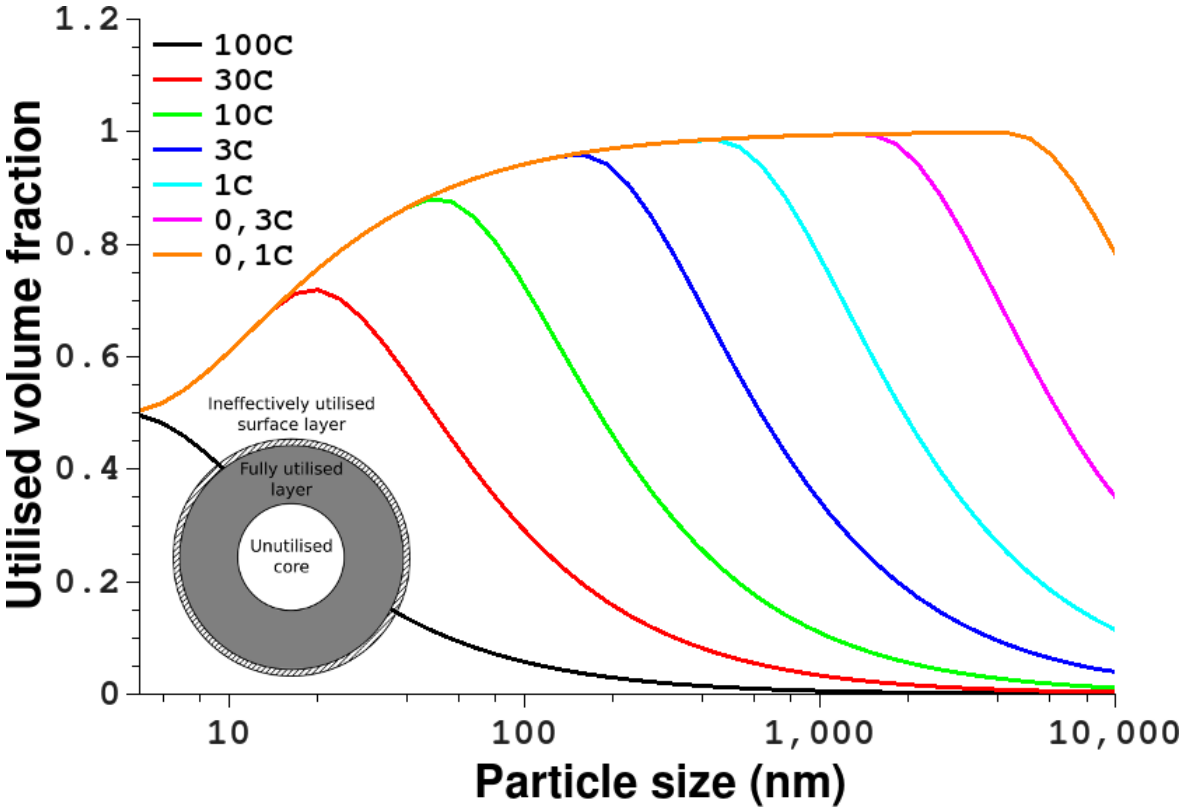

Figure 24: Theoretical utilisation of a electrolyte crystallite volume for lithium intercalation reactions as a function of the cycling rate. Surface layer thickness of 2 nm, surface layer utilisation of 50%, and linear advancement of a intercalation front at a speed of 200 nm/h were assumed.

4.2.2 Effect of conductive doping

In paper IV it was also found out that the introduction of a conductive metal (Ag, Cu) as a dopant to the LTO synthesis resulted in an improvement in the specific capacity, especially at high C-rates (Figure 25). The silver doping of the 40 nm $Li_4Ti_5O_{12}$ nanoparticles provided an improvement of 12% compared to the undoped particles at a C-rate of 10. This improvement in the performance at high currents can be attributed to improved electrical conductivity of the material due to the silver doping.

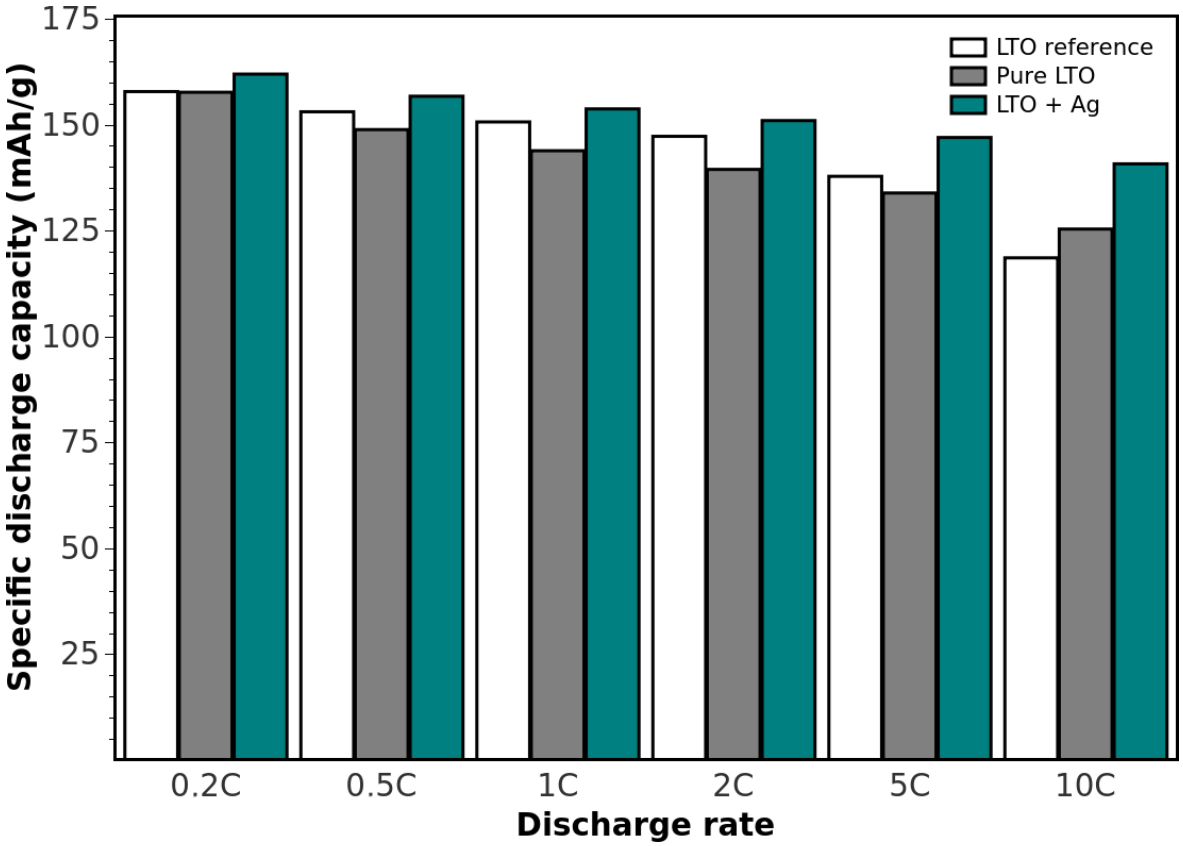

Figure 25: Specific capacity as a function of discharge rate for Li-ion half-cells with negative electrode containing $Li_4Ti_5O_{12}$ synthesised using the high-temperature FSP set-up. (Based on results presented in Paper IV)

It is likely that the main effect of the doping would be in the step 2 of the simple diffusion model illustrated in the Figure 23. In effect the silver doping would provide additional conduction pathways for the electrons from the current collector to the charge transfer site.

However, this would not explain the small improvement in the specific capacity seen at low C-rates for the silver doped material (0.2C in Figure 25). It is possible that the silver acts as a surface passivation layer for the $Li_4Ti_5O_{12}$ particles reducing necking effect at the point of contact between the particles. Or it might be that the silver nanoparticles somehow act as catalysts for the charge transfer reaction. This, however, is not clear from the present data and will require further research.

If the $Li_4Ti_5O_{12}$ synthesised here is compared to recently published commercial $Li_4Ti_5O_{12}$ (nCCVC-LTO) (Venugopal et al., 2010) its electrochemical performance is found to be very promising. Figure 26 shows a comparison of the discharge capacity of the pure and silver doped LTOs with the nCCVC-LTO at various C-rates. From this it is clear that the nanoparticulate LTO presented in Paper IV outperforms the commercial product in both cyclability and high-current operation. Specifically the silver doped $Li_4Ti_5O_{12}$ has 99.8% of the capacity left at the 5th cycle versus 94.0% for the nCCVC-LTO, and 91.4% versus 62.4% at 10C.

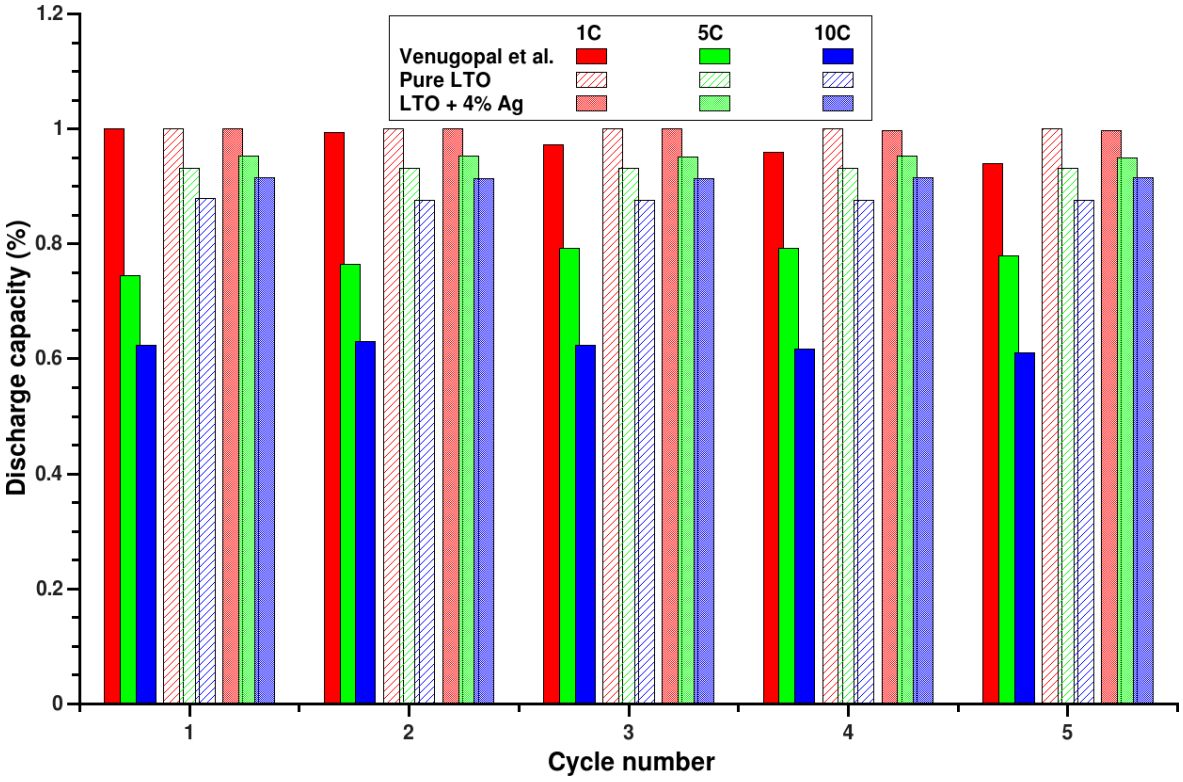

Figure 26: Relative discharge capacity of Li-ion half-cells with HT-LTO nanoparticles compared to recently published commercial product at various C-rates. (Data for commercial product reproduced from Venugopal et al. (2010))

The significant drop in the high-current capacity observed for the nCCVC-LTO is similar to that found for $Li_4Ti_5O_{12}$ nanoparticles synthesised with the traditional flame spray pyrolysis method as discussed in Paper IV. It was deduced that the likely cause of the poor performance in that case was the rapid quenching and dilution of the synthesised aerosol. This stops the growth of primary particles, and the reorganisation of crystallite domains within the particles, resulting in large volume fraction of poorly utilised surface, or boundary, regions as discussed above and illustrated in Figure 24.

5 Conclusions

The aerosol route for the synthesis of nanoparticles has been found to be simple and efficient, and it is already employed on several applications (Gurav et al., 1993; Das and Ansari, 2009; Pratsinis, 2010). However, its utilisation in the field of energy technology is only now gathering speed. It has been shown here that various nanomaterials can be synthesised using spray pyrolysis and flame spray pyrolysis, and that the material properties can be tuned by altering the process conditions, such as reaction atmosphere, temperature, residence time, and stoichiometry.

Furthermore, it was shown that the properties of the synthesised particles have significant impacts on their utility in the chosen application. As such the synthesis process and parameters can be chosen in such a way as to optimise the product material for a given application.

Specifically, it was illustrated that gold nanoparticles of less than 5 nm in size can be synthesised in a simple spray pyrolysis process. A designed homoleptic organometal was used as the gold precursor in organic solvent. It was found that in the heated reaction zone the evaporating droplets acted as microreactors. The decomposition of the precursor within the droplets lead to a formation of surface stabilised gold nanoparticles. This nano-gold material could find use in catalytic or optical application, or could provide surface plasmon resonance for e.g. surface-enhanced Raman spectroscopy (Lee and Meisel, 1982; Wu et al., 2008; de la Garza et al., 2010; Zhou et al., 2011).

The spray pyrolysis method was found to be very flexible in the choice precursor material. On the opposite site of the range from the designer gold precursor was an industrial by-product iron sulphate used in the synthesis of $LiFePO_4$ nanoparticles. This proof-of-concept study highlighted the relationship between the synthesis conditions (temperature, residence time, oxidative potential and stoichiometry) and the product properties (purity, crystalline polymorph, and particle morphology).

Finally, it was shown that nanoparticulate $Li_4Ti_5O_{12}$ with electrochemical performance superior to available alternatives can be easily synthesised using the flame spray synthesis route. To achieve the optimal material properties careful control of the synthesis conditions, particularly the residence time, was required.

The $Li_4Ti_5O_{12}$/$LiFePO_4$ form a pair of electrode materials with very promising properties for certain energy storage applications. Their precursor materials are abundant

and easily available, as well as environmentally benign. This makes the materials easy to produce handle and recycle, or dispose of. Furthermore, both have been shown to be extremely stable in Li-ion cells making a battery utilising them potentially very long lasting. Such a battery would also be safe to use as the intercalation potentials of the two electrodes are with in the stability window of the commonly used electrolytes.

In addition, when the particle size of the electrode is reduced to the nanoscale the resulting high surface area enables high current operation of the batteries. Unfortunately however, the materials have a relatively low specific capacity and reducing the particle size can further reduce this, thus requiring a compromise between capacity and current.

As such the pair would be best suited to static battery application where reliability and long life time are paramount, such as evening the power output of solar cells or wind turbines. Alternatively, it could find use in automotive solutions where high peak power output is more important than high energy density, for example electric construction machinery or electric buses utilising regular top-up charging.

Optimisation of the nanomaterials for these applications would require further research. In particular, in this work the role of the electrolyte has not been studied. In addition for the synthesis methods to be useful in industrial production they need to be scaled up from the laboratory scale. Thus the next step in this research should be testing the synthesis of the LTO and the LFP in the pilot scale flame spray pyrolysis set-up and optimising the process parameters to get the best possible product for the application.

Furthermore, knowledge of the molecular processes within the FSP flame are not yet well understood and would need further study. This would then enable better prediction of the effects of changes in the process parameters and the precursor materials on the synthesised nanoparticle properties.

6 Review of papers and the author's contribution

The research presented here was carried out at the Fine Particle and Aerosol Technology Laboratory in the University of Eastern Finland in the period 2010–2016 under the supervision of Professor Jorma Jokiniemi and Docent Anna Lähde.

Paper I describes a spray pyrolysis method for the synthesis of gold nanoparticles using spray pyrolysis type reactor. Droplets of gold precursor solution, with homoleptic organometallic gold clusters in ethanol or hexane, underwent rapid evaporation within a heated laminar flow furnace. This resulted in the droplets to function as microreactors for the formation of clusters of gold nanoparticles.

The author was responsible for the X-ray diffraction measurements, and the analysis of crystalline phases and crystallite sizes. In addition, the design of the experimental set-up, the nanoparticle synthesis, the Raman spectroscopic studies, and the manuscript preparation was carried out by A. Lähde in collaboration with T. Torvela and the author. The work was supervised by J. Jokiniemi

Paper II describes a spray pyrolysis method for the synthesis of $LiFePO_4$ nanoparticles from low-cost precursor materials. The study resulted in a proof-of-concept for the utilisation of an industrial by-product $FeSO_4 \cdot 7\,H_2O$ as iron precursor in the synthesis of $LiFePO_4$ nanoparticles. The spray pyrolysis method was used to generate the nanoparticles from an aqueous precursor solution. The study highlighted the importance of the process parameters on the properties of the product particles. In this case, sufficient residence time at 800°C in slightly reducing atmosphere was found to be optimal.

The author was the principal investigator of the paper, in charge of the experimental design, and material synthesis and analyses, apart from for the electron microscopy conducted by T. Torvela. The manuscript was prepared by the author in collaboration with T. Torvela, J. Jokiniemi, and A. Lähde.

Paper III describes a flame spray pyrolysis method for the synthesis of pure and doped $Li_4Ti_5O_{12}$ nanoparticles. Organometallic precursors dissolved into organic solvent resulted in formation of elemental and phase pure $Li_4Ti_5O_{12}$ nanoparticles with average crystallite and primary particle size of 10 nm. Furthermore, it was shown that conductive doping with copper or silver could be carried out simultaneously to the

synthesis. However, the resulting composites were found to have significantly differing structures. While a separate phase of metallic silver formed onto the LTO particles, the copper reacted to form $Li_2CuTi_3O_8$ in solid solution with the $Li_4Ti_5O_{12}$.

The author was the coordinator of the study together with J. Jokiniemi, and carried out the experimental design and material synthesis in collaboration with R. Büchel, O. Waser, and J. Leskinen. The material analyses were conducted by the author together with A. Lähde, J. Leskinen, and U. Tapper. The manuscript was prepared together with the co-authors.

Paper IV describes a modified flame spray pyrolysis method for the synthesis of pure and doped $Li_4Ti_5O_{12}$ nanoparticles and their electrochemical performance in Li-ion half cells. The LTO nanoparticles prepared with the traditional FSP method were found to perform poorly in Li-ion battery application, likely due to their very small crystallite size. To encourage crystallite growth a flow furnace was added to the synthesis apparatus. This increased the high-temperature residence time of the particles from about 1 ms to 1 s and the crystallite size form about 10 nm to 40 nm. As a result significant improvements in the electrochemical performance of the nanomaterial was observed. At low current densities the specific capacity was equal or greater than that for a commercial reference for the pure and doped LTO, respectively. However, at high current densities they exceeded the reference by 6 and 19%, respectively.

The author coordinated the study together with J. Jokiniemi and U. Lassi. The material synthesis and characterisation were carried out by the author in collaboration with A. Lähde and T. Torvela, while the electrochemical measurements and analysis were performed together with J. Välikangas.

References

Arai, Y., editor (1996). *Chemistry of Powder Production*. Chapman & Hall, London, 1 edition.

Atkins, P. W., editor (1990). *Physical chemistry*. Oxford University Press, Oxford, 4 edition.

Bale, C., Chartrand, P., Degterov, S., Eriksson, G., Hack, K., Mahfoud, R. B., Melançon, J., Pelton, A., and Petersen, S. (2002). Factsage thermochemical software and databases. *Calphad*, 26(2):189–228.

Brunauer, S., Emmett, P. H., and Teller, E. (1938). Adsorption of gases in multimolecular layers. *Journal of the American Chemical Society*, 60(2):309–319.

Buesser, B. and Pratsinis, S. E. (2012). Design of nanomaterial synthesis by aerosol processes. *Annual Review of Chemical and Biomolecular Engineering*, 3:103–127.

Chang, W., Skandan, G., Hahn, H., Danforth, S. C., and Kear, B. H. (1994). Chemical vapor condensation of nanostructured ceramic powders. *Nanostructured Materials*, 4(3):345–351.

Das, I. and Ansari, S. A. (2009). Nanomaterials in science and technology. *Journal of Scientific & Industrial Research*, 68(8):657–667.

de la Garza, M., Hernándeza, T., Colásb, R., and Gómez, I. (2010). Deposition of gold nanoparticles on glass substrate by ultrasonic spray pyrolysis. *Materials Science and Engineering: B*, 174(1–3):9–12.

Donahue, N. M., Robinson, A. L., and Pandis, S. N. (2009). Atmospheric organic particulate matter: From smoke to secondary organic aerosol. *Atmospheric Environment*, 43(1):94–106.

du Pasquier, A., Plitz, I., Menocal, S., and Amatucci, G. (2003). A comparative study of Li-ion battery, supercapacitor and nonaqueous asymmetric hybrid devices for automotive applications. *Journal of Power Sources*, 115(1):171–178.

Fang, J., Nakamura, H., and Maeda, H. (2011). The epr effect: Unique features of tumor blood vessels for drug delivery, factors involved, and limitations and augmentation of the effect. *Advanced Drug Delivery Reviews*, 63(3):136–151.

Fotou, G. P., Kodas, T. T., and Anderson, B. (2000). Coating titania aerosol particles with zro_2, al_2o_3/zro_2, and sio_2/zro_2 in a gas-phase process. *Aerosol Science and Technology*, 33(6):557–571.

Friedlander, S. K., editor (2000). *Smoke, Dust, and Haze: Fundamentals of Aerosol Dynamics*. Oxford University Press, New York, 2 edition.

Gracia-Pinilla, M., Martínez, E., Vidaurri, G. S., and Pérez-Tijerina, E. (2010). Deposition of size-selected cu nanoparticles by inert gas condensation. *Nanoscale Research Letters*, 5(1):180–188.

Gröhn, A. J., Pratsinis, S. E., Sánchez-Ferrer, A., Mezzenga, R., and Wegner, K. (2014). Scale-up of nanoparticle synthesis by flame spray pyrolysis: The high-temperature particle residence time. *Industrial and Engineering Chermistry Research*, 53(26):10734–10742.

Gurav, A., Kodas, T., Pluym, T., and Xiong, Y. (1993). Aerosol processing of materials. *Aerosol Science and Technology*, 19(4):411–452.

Hampden-Smith, M. J., Kodas, T. T., Powell, Q. H., Skamser, D. J., Caruso, J., and Chandler, C. D. (2006). Aerosol method and apparatus, particulate products, and electronic devices made therefrom.

Hinds, W. C., editor (1999). *Aerosol Technology: Properties, Behaviour, and Measurement of Airborne Particles*. John Wiley & Sons, Inc., New York, 2 edition.

Hosokawa, M., Nogi, K., Naito, M., and Yokoyama, T., editors (2008). *Nanoparticle Technology Handbook*. Elsevier, Amsterdam, 1 edition.

Huang, S., Wen, Z., Zhang, J., and Yang, X. (2007). Improving the electrochemical performance of $Li_4Ti_5O_{12}$/Ag composite by an electroless deposition method. *Electrochimica Acta*, 52(11):3704–3708.

Jhu, C.-Y., Wang, Y.-W., Wen, C.-Y., and Shu, C.-M. (2012). Thermal runaway potential of licoo2 and li(ni1/3co1/3mn1/3)o2 batteries determined with adiabatic calorimetry methodology. *Applied Energy*, 100:127–131.

Kammler, H. K., Mädler, L., and Pratsinis, S. E. (2001). Flame synthesis of nanoparticles. *Chemical Engineering and Technology*, 24(6):583–596.

Kavan, L., Prochazka, J., Spitler, T. M., Kalbac, M., Zukalova, M., Drezen, T., and Gratzel, M. (2003). Li insertion into $Li_4Ti_5O_{12}$ (spinel). *Journal of the Electrochemical Society*, 150(7):A1000–A1007.

Kodas, T. T. and Hampden-Smith, M., editors (1999). *Aerosol processing of materials*. Wiley-VCH, New York, 1 edition.

Kruis, F. E., Fissan, H., and Peled, A. (1998). Synthesis of nanoparticles in the gas phase for electronic, optical and magnetic applications – a review. *Journal of Aerosol Science*, 29(5–6):511–535.

Lähde, A., Kokkonen, N., Karttunen, A. J., Jääskeläinen, S., Tapper, U., Pakkanen, T. A., and Jokiniemi, J. (2011). Preparation of copper-silicon dioxide nanoparticles with chemical vapor synthesis. *Journal of Nanoparticle Research*, 13(9):3591–3598.

Lähde, A., Raula, J., and Kauppinen, E. I. (2008). Deposition of size-selected cu nanoparticles by inert gas condensation. *International Journal of Pharmaceutics*, 358(1–2):256–262.

Lee, P. C. and Meisel, D. (1982). Adsorption and surface-enhanced raman of dyes on silver and gold sols. *Journal of Physical Chemistry*, 86(17):3391–3395.

Lehtinen, K. E. J., Windeler, R. S., and Friedlander, S. K. (1996). A note on the growth of primary particles in agglomerate structures by coalescence. *Journal of Colloid and Interface Science*, 182(2):606–608.

Lu, A.-H., Salabas, E. L., and Schüth, F. (2007). Magnetic nanoparticles: Synthesis, protection, functionalization, and application. *Angewandte Chemie International Edition*, 46(8):1222–1244.

Luther, W. and Zweck, A., editors (2013). *Safety aspects of engineered nanomaterials*. CRC Press, Boca Raton, 1 edition.

Lyyränen, J., Jokiniemi, J., Kauppinen, E. I., Backman, U., and Vesala, H. (2004). Comparison of different dilution methods for measuring diesel particle emissions. *Aerosol Science and Technology*, 38(1):12–23.

Ma, R., Levard, C., Michel, F. M., G. E. Brown, J., and Lowry, G. V. (2013). Sulfidation mechanism for zinc oxide nanoparticles and the effect of sulfidation on their solubility. *Environmental Science & Technology*, 47(6):2527–2534.

Mädler, L. and Friedlander, S. K. (2007). Transport of nanoparticles in gases: Overview and recent advances. *Aerosol and Air Quality Research*, 7(3):304–342.

Mädler, L., Kammler, H. K., Mueller, R., and Pratsinis, S. E. (2002). Controlled synthesis of nanostructured particles by flame spray pyrolysis. *Journal of Aerosol Science*, 33(2):369–389.

Miettinen, M., Hokkinen, J., Karhunen, T., Torvela, T., Pfüller, C., Ramsteiner, M., Tapper, U., Auvinen, A., Jokiniemi, J., and Lähde, A. (2014). Synthesis of novel carbon nanostructures by annealing of silicon-carbon nanoparticles at atmospheric pressure. *Journal of Nanoparticle Research*, 16(1):ID 2168.

Mäkelä, J. M., Keskinen, H., Forsblom, T., and Keskinen, J. (2004). Generation of metal and metal oxide nanoparticles by liquid flame spray process. *Journal of Materials Science*, 39(8):2783–2788.

Nel, A., Xia, T., Mädler, L., and Li, N. (2006). Toxic potential of materials at the nanolevel. *Science*, 311(5761):622–627.

Oberdörster, G., Oberdörster, E., and Oberdörster, J. (2005). Nanotoxicology: an emerging discipline evolving from studies of ultrafine particles. *Environmental Health Perspectives*, 113(7):823–830.

Ohzuku, T., Ariyoshi, K., Yamamoto, S., and Makimura, Y. (2001). A 3-volt lithium-ion cell with li[ni$_{1/2}$mn$_{3/2}$]o$_4$ and li[li$_{1/3}$ti$_{5/3}$]o$_4$: A method to prepare stable positive-electrode material of highly crystallized li[ni$_{1/2}$mn$_{3/2}$]o$_4$. *Chemistry Letters*, 30(12):1270–1271.

Ohzuku, T., Ueda, A., and Yamamoto, N. (1995). Zero-strain insertion materials of Li[Li$_{1/3}$Ti$_{5/3}$]O$_4$ for rechargeable lithium cells. *Journal of the Electrochemical Society*, 142(5):1431–1435.

Panero, S., Satolli, D., and Scrosati, M. S. B. (2000). A new type of lithium-ion cell based on the li4ti5o12/li2co0.4fe0.4mn3.2o8 high-voltage, electrode combination. *Electrochemistry Communications*, 2(11):810–813.

Park, M., Zhang, X., Chung, M., Less, G. B., and Sastry, A. M. (2010). A review of conduction phenomena in li-ion batteries. *Journal of Power Sources*, 195(24):7904–7929.

Pitkethy, M. J. (2003). Nanoparticles as building blocks? *Materials Today*, 6(12, Supplement):36–42.

Porstendörfer, J., Scheibel, H. G., Pohl, F. G., Preining, O., Reischl, G., and Wagner, P. E. (1985). Heterogeneous nucleation of water vapor on monodispersed ag and nacl particles with diameters between 6 and 18 nm. *Aerosol Science and Technology*, 4(1):65–79.

Pratsinis, S. E. (1998). Flame aerosol synthesis of ceramic powders. *Progress in Energy and Combustion Science*, 24(3):197–219.

Pratsinis, S. E. (2010). Aerosol-based technologies in nanoscale manufacturing: from functional materials to devices through core chemical engineering. *AIChE Journal*, 56(12):3028–3035.

Qin, X., Wang, X., Xiang, H., Xie, J., Li, J., and Zhou, Y. (2010). Mechanism for hydrothermal synthesis of lifepo4 platelets as cathode material for lithium-ion batteries. *Journal of Physical Chemistry C*, 114(39):16806–16812.

Realea, P., Paneroa, S., Scrosatia, B., Garcheb, J., Wohlfahrt-Mehrensb, M., and Wachtlerb, M. (2004). A safe, low-cost, and sustainable lithium-ion polymer battery. *Journal of the Electrochemical Society*, 151(12):A2138–A2142.

Rodriguez, J. A., Jirsak, T., Chaturvedi, S., and Dvorak, J. (2001). Chemistry of so2 and no2 on zn(0001)-zn and zno powders: Changes in reactivity with surface structure and composition. *Journal of Molecular Catalysis A: Chemical*, 167(1–2):47–57.

Ruusunen, J., Pyykönen, J., Ihalainen, M., Tiitta, P., Torvela, T., Karhunen, T., Sippula, O., Qin, Q. H., van Dijken, S., Joutsensaari, J., Lähde, A., and Jokiniemi, J. (2015). A novel porous tube reactor for nanoparticle synthesis with simultaneous gas-phase reaction and dilution. *Aerosol Science and Technology*, 49(11):1170–1180.

Scrosati, B. and Garche, J. (2010). Lithium batteries: Status, prospects and future. *Journal of Power Sources*, 195(9):2419–2430.

Seinfield, J. H. and Pandis, S. N., editors (1998). *Atmospheric Chemistry and Physics: From Air Pollution to Climate Change*. John Wiley & Sons, Inc., New York, 1 edition.

Sippula, O., Koponen, T., and Jokiniemi, J. (2012). Behaviour of alkali metal aerosol in high-temperature porous tube sampling probe. *Aerosol Science and Technology*, 46(10):1151–1162.

Spurny, K. R., editor (2000). *Aerosol Chemical Processes in the Environment*. CRC Press LLC, Boca Raton, 1 edition.

Strobel, R. and Pratsinis, S. E. (2007). Flame aerosol synthesis of smart nanostructured materials. *Journal of Materials Chemistry*, 17:4743–4756.

Sun, Y., Zhang, J.-P., Yang, G., and Li, Z.-H. (2007). Preparation of activated carbon with large specific surface area from reed black liquor. *Environmental Technology*, 28(5):491–497.

Swihart, M. T. (2003). Vapor-phase synthesis of nanoparticles. *Current Opinion in Colloid & Interface Science*, 8(1):127–133.

Tjong, S. and Chen, H. (2004). Nanocrystalline materials and coatings. *Materials Science and Engineering R: Reports*, 45(1–2):1–88.

Venugopal, G., Hunt, A., and Alamgir, F. (2010). Nanomaterials for energy storage in lithium-ion battery applications. *Material Matters*, 5(2):42–45.

Wang, D., Xu, H.-Y., Gu, M., and Chen, C.-H. (2009). $Li_2CuTi_3O_8$–$Li_4Ti_5O_{12}$ double spinel anode material with improved rate performance for li-ion batteries. *Electrochemistry Communications*, 11(1):50–53.

Wang, Z. L. (2004). Zinc oxide nanostructures: growth, properties and applications. *Journal of Physics: Condensed Matter*, 16(25):R829–R858.

Waser, O., Büchel, R., Hintennach, A., Novák, P., and Pratsinis, S. E. (2011). Continuous flame aerosol synthesis of carbon-coated nano-lifepo$_4$ for li-ion batteries. *Journal of Aerosol Science*, 42(10):657–667.

Wu, D.-J., Xu, X.-D., and Liu, X.-J. (2008). Tunable near-infrared optical properties of three-layered metal nanoshells. *Journal of Chemical Physics*, 129(7):ID 074711.

Yoshio, M., Brodd, R. J., and Kozawa, A., editors (2009). *Lithium-Ion Batteries: Science and Technologies*. Springer-Verlag, New York, 1 edition.

Zhou, Z.-K., Peng, X.-N., Yang, Z.-J., Zhang, Z.-S., Li, M., Su, X.-R., Zhang, Q., Shan, X., Wang, Q.-Q., and Zhang, Z. (2011). Tuning gold nanorod-nanoparticle hybrids into plasmonic fano resonance for dramatically enhanced light emission and transmission. *Nano Letters*, 11(1):49–55.